

Microphysical features of typhoon and non-typhoon rainfall observed in Taiwan, an island in the northwest Pacific.

Jayalakshmi Janapati¹, Balaji Kumar Seela¹, Pay-Liam Lin^{1,2,3*}, Meng-Tze Lee⁴, Everett Joseph⁵

¹Institute of Atmospheric Physics, Department of Atmospheric Sciences, National Central University, Zhongli district, Taoyuan city, Taiwan

²Earthquake-Disaster & Risk Evaluation and Management Center, National Central University, Zhongli district, Taoyuan city, Taiwan.

³Research Center for Hazard Mitigation and Prevention, National Central University, Zhongli district, Taoyuan City, Taiwan

⁴Department of Atmospheric and Oceanic Sciences, McGill University, Montreal, Quebec, Canada

⁵National Center for Atmospheric Research, Boulder, Colorado

***Correspondence to:**

Prof. Pay-Liam Lin

Institute of Atmospheric Physics, Department of Atmospheric Sciences

National Central University, Zhongli district, Taoyuan City, Taiwan

Phone: 03-422-3294 03-422-7151 ext. 65509

E-mail: pliam@pblap.atm.ncu.edu.tw

Formatted: Default Paragraph Font, Font: (Default) +Body (Calibri), 11 pt

2 Abstract.

3 Information about the raindrop size distribution (RSD) is vital to comprehend the
4 precipitation microphysics, improve the rainfall estimation algorithms, and appraise the rainfall
5 erosivity. Previous research has revealed that the RSD exhibits diversity with geographical
6 location and weather type, which perpetrates to assess the region and weather-specific RSDs.
7 Based on long-term (2004 to 2016) disdrometer measurements in north Taiwan, this study
8 pursued to demonstrate the RSD aspects of summer seasons that were bifurcated into two
9 weather-~~systems~~ [conditions](#), namely typhoon (TY) and non-typhoon (NTY) rainfall. The results
10 show a higher concentration of small drops and a lower concentration of big-size drops in TY
11 compared to NTY rainfall, and this behavior persisted even after characterizing the RSDs into
12 different rainfall rate classes. RSDs expressed in gamma parameters show higher mass-weighted
13 mean diameter (D_m) and lower normalized intercept parameter (N_w) values in NTY than TY
14 rainfall. Forbye, sorting of these two weather ~~systems~~ [conditions](#) (TY and NTY rainfall) into
15 stratiform and convective regimes did reveal a large D_m in NTY than the TY rainfall. The RSD
16 empirical relations used in the valuation of rainfall rate ($Z-R$, D_m-R , and N_w-R) and rainfall
17 kinetic energy ($KE-R$, and $KE-D_m$) were enumerated for TY and NTY rainfall, and they
18 exhibited profound diversity between these two weather-~~systems~~ [conditions](#). Attributions of RSD
19 variability between the TY and NTY rainfall to the thermo-dynamical and microphysical
20 processes are elucidated with the aid of reanalysis, remote-sensing, and ground-based datasets.

21

22 **Keywords:** typhoons, non-typhoons, disdrometer, rainfall kinetic energy, north Taiwan

23

24

25 **1. Introduction**

26 Taiwan, an island in the northwest Pacific, has complex topography with an outspread
27 from south to north, with an average elevation of about 2 km and peaks of ~ 4 km. The East
28 China Sea bounds Taiwan in the north, the Philippine Sea in the east, Luzon Strait in the south,
29 and the South China Sea in the southwest. This island is affected by two monsoon regimes:
30 southwesterly monsoon (May to August) and northeasterly monsoon (September to April), and
31 these two monsoon regimes were further categorized into winter (December to February), spring
32 (March to April), mei-yu (mid-May to mid-June), summer (mid-June to August), typhoon (May
33 to October), and autumn (September to November) seasons (Chen and Chen, 2003). Among the
34 above-mentioned seasons, the summer seasons, exclusively associated with thunderstorms and
35 typhoons, have intense precipitation than other seasons. Despite reports on the rainfall
36 individualities of different seasons and weather systems in Taiwan (Chen et al., 1999; Chen et al.,
37 2007; Chen et al., 2010; Chen and Chen, 2011; Liang et al., 2017; Tu and Chou, 2013), few
38 attempts were made to explicate rain microphysical aspects, exclusively the RSD characteristics.

39
40 The RSDs aid in diverse fields like meteorology, hydrology and remote sensing, and
41 afford an insight into the precipitation microphysics (Rosenfeld and Ulbrich, 2003).
42 Characterization of RSDs offers the opportunity to design radar rainfall estimation algorithms
43 (Ryzhkov and Zrnić, 1995), improve the cloud modeling parameterization (McFarquhar et al.,
44 2015), assess the rainfall erosivity relations (Janapati et al., 2019), validate the remote sensing
45 instruments (Liao et al., 2014; Nakamura and Iguchi, 2007), and appraise the rain attenuations
46 (Chen et al., 2011). Owing to the aforementioned implications of RSDs, ample literature exists
47 on RSDs for spatial, seasonal (Thompson et al., 2015; Jayalakshmi and Reddy, 2014; Seela et al.,

Field Code Changed

Field Code Changed

Field Code Changed

Field Code Changed

Field Code Changed

Field Code Changed

Field Code Changed

Field Code Changed

Field Code Changed

48 2017;Seela et al., 2018;Krishna et al., 2016;Seela et al., 2016) variations, storm to storm, within
49 the storm (Kumari et al., 2014;Maki et al., 2001;Jung et al., 2012;Bao et al., 2020;Janapati et al.,
50 2017), and different precipitations (Tokay and Short, 1996;Krishna et al., 2016).

Field Code Changed

Field Code Changed

51
52 Investigations on RSDs have been escalating to illuminate the hydrological (Lin and
53 Chen, 2012;Lu et al., 2008;Janapati et al., 2019;Chang et al., 2017) and microphysical
54 characteristics (Chu and Su, 2008;Jung et al., 2012;Seela et al., 2017;Seela et al., 2018;Lee et al.,
55 2019;Janapati et al., 2020) of diverse precipitating clouds in Taiwan. For instance, Chu and Su
56 (2008) reconnoitered the slope-shape relations for seven precipitation events related to four
57 different weather systems in north Taiwan, and they showed that the derived μ - Λ relation was
58 independent of the gamma RSD moment order. Measurements of a squall line in south Taiwan
59 with ground-based radar and disdrometer revealed that the D_m values in the squall line's
60 convective precipitation were higher than the maritime clusters (Jung et al., 2012). Chang et al.
61 (2009) analyzed the RSDs of landfall typhoons in north Taiwan, and they opinioned that the
62 interaction of typhoons with Taiwan's complex terrain resulted in the RSDs intermediate to
63 maritime and continental clusters. The comparison study of summer seasons' RSDs between
64 Taiwan and Palau Islands by Seela et al. (2017) revealed more large drops in Taiwan than Palau,
65 and they contended that deeply extended convective clouds with more aerosols in Taiwan
66 resulted in the differences between these two Islands. With the aid of long-term disdrometer
67 measurements for summer and winter seasons in north Taiwan, Seela et al. (2018) noticed a
68 profound disparities in RSDs between these two seasons, and they established the attribution of
69 RSDs differences to the microphysical processes concomitant with deep convective clouds in
70 summer and warm clouds in winter. Furthermore, investigations on microphysical features of six

Field Code Changed

Field Code Changed

Field Code Changed

Field Code Changed

Field Code Changed

Field Code Changed

Field Code Changed

71 seasons (winter, spring, mei-yu, summer, typhoon, and autumn) in north Taiwan divulged the
72 highest mean D_m values in the summer and highest concentration ($\log_{10}N_w$) in the winter (Lee et
73 al., 2019). A recent study on Indian and Pacific Ocean tropical cyclones manifested higher D_m
74 values in Pacific Ocean tropical cyclones than the Indian Ocean tropical cyclones (Janapati et al.,
75 2020).

Field Code Changed

Field Code Changed

76
77 Efforts have been performed to reveal the RSDs characteristics of tropical cyclones and
78 non-tropical cyclones in India, Australia, China, and Japan (Radhakrishna and Narayana Rao,
79 2010;Kumar and Reddy, 2013;Deo and Walsh, 2016;Chen et al., 2019;Chen et al., 2017).
80 Analysis of tropical cyclones and non-tropical cyclones RSDs in Gadanki (Radhakrishna and
81 Narayana Rao, 2010) and Kadapa (Kumar and Reddy, 2013) unveiled a higher concentration of
82 small drops in tropical cyclones than the non-tropical cyclones. In Australia, Deo and Walsh
83 (2016) illustrated the tropical cyclones and non-tropical cyclones RSDs and demonstrated higher
84 D_m values in non-tropical cyclones than tropical cyclones rainfall. From the 2DVD
85 measurements in East china, Chen et al. (2017) appraised the polarimetric radar variables for
86 typhoons, Mei-yu, and squall line precipitations, and they revealed discrete alterations among
87 these weather systems. Over south China, distinct differences in rain integral parameters of
88 typhoons and squall lines were perceived by Zhang et al. (2019), and they concluded that it is
89 essential to adopt precipitation specific rainfall estimators. Examination of typhoons and mei-yu
90 season RSDs in Japan affirmed maritime behavior in typhoons and continental behavior in mei-
91 yu rainfall (Chen et al., 2019).

Field Code Changed

Field Code Changed

Field Code Changed

Field Code Changed

Field Code Changed

Field Code Changed

Field Code Changed

93 In contempt of investigations on the typhoon and non-typhoon weather
94 conditions'~~weather-systems'~~ rainfall characteristics (Chen and Chen, 2011; Tu and Chou, 2013),
95 the microphysical features, especially the summer seasons' RSDs (explicitly segregated to
96 typhoon and non-typhoon weather conditions~~weather-systems~~) are yet to be documented for the
97 Taiwan region. On this account, this study sought to address the following objectives: 1. To
98 investigate alike or unlike individualities of RSDs between the typhoon and non-typhoon
99 rainfall, 2. To identify comparable/unrelated features of typhoon and non-typhoon rainfall to the
100 previous studies, 3. quantification of rainfall rate and rainfall kinetic energy relations, 4. To
101 discern conceivable rationale for peculiarities in the RSDs between typhoon and non-typhoon
102 rainfall events. In this context, to address the aforementioned objectives for the typhoons and
103 non-typhoons rainfall, long-term disdrometer, radar, remote-sensing, and re-analysis data sets
104 were used.

Field Code Changed

106 2. Data sets used

107 Taiwan geographic map with National Central University (NCU) (24° 58' N, 121° 10' E)
108 site (indicated with a filled green circle), where the Joss–Waldvogel disdrometer (JWD) (Joss
109 and Waldvogel, 1969) measurements were conducted [for the summer season (16 June to -31
110 August) rainy days of the years 2004 to 2016], is shown in Fig.1. The disdrometer measurements
111 in summer seasons were further classified into a typhoon (TY) and non-typhoon (NTY) regimes.
112 In identifying the rainfall amounts of typhoons over Taiwan, previous studies adopted different
113 criteria (Tu and Chou, 2013; Chu et al., 2007; Chen et al., 2010). For instance, if a typhoon center
114 was invaded the rectangular grid box of 21°-26° N and 119°-125° E (Chu et al., 2007) or 19.5°-
115 27.5° and 117.5°-124.5° E (Chen et al., 2010) or 18°-29.5° N and 116°-126° E (Tu and Chou,

Field Code Changed

Field Code Changed

Field Code Changed

Field Code Changed

Field Code Changed

116 2013), the corresponding rain in Taiwan was selected as typhoon induced rain. On the other
117 hand, in the current study, precipitation at the NCU disdrometer site was considered as typhoon-
118 induced rain when the typhoon center was ≤ 500 km from the disdrometer (Janapati et al., 2019),
119 and the rest of the rainy days in summer seasons were categorized as NTY rainy days. With this
120 condition, a total number of 59 TY rainy days (hereafter TY days) and 131 NTY rainy days
121 (hereafter NTY days) were recorded by the NCU JWD from 2004 to 2016 (excluding 2008 and
122 2009 years).

Field Code Changed

123
124 The JWD has its advantage and disadvantages over the other disdrometers (Lee and
125 Zawadzki, 2005;McFarquhar and List, 1993;Sauvageot and Lacaux, 1995;Sheppard,
126 1990;Sheppard and Joe, 1994;Tokay et al., 2001;Tokay et al., 2013). For instance, JWD can't
127 measure fall velocity; hence, to evaluate the RSD parameters from the JWD, we assumed that
128 raindrops reach the ground with terminal velocity. Further, in heavy rainfall events, the JWD
129 measures the spurious values for the raindrops of diameter < 1 mm, and it was named as the
130 dead-time of the instrument. To deal with the dead-time of the JWD, the manufacturer provided
131 an error correction multiplication matrix based on a correction scheme from Sheppard and Joe
132 (1994). However, as the JWD can't record any drops for the first three to four channels in heavy
133 rainfall events, the multiplicative matrix algorithm does not increase the counts when the channel
134 has no drops (Tokay & Short, 1996; Tokay et al., 2001); hence, in this study, we didn't apply the
135 dead-time correction to the JWD data. On top of that, 1-min RSD samples with raindrops count $<$
136 10 and rainfall rate $< 0.1 \text{ mm h}^{-1}$ were discarded (Tokay & Short, 1996). The daily rainfall
137 accumulations from the JWD are related to the collocated rain gauge for both TY and NTY rain
138 regimes and are illustrated with scatter plots in Fig.2. ~~Strong correlations between JWD and rain~~

Field Code Changed

Field Code Changed

139 ~~gauge measurements for both TY and NTY days provide the trustworthiness of the JWD data for~~
 140 ~~further analysis. The rainy days (TY: 04 days and NTY: 0 days) with larger discrepancy between~~
 141 ~~JWD and rain gauge measurements were discarded in this study. Further, we compared the JWD~~
 142 ~~measurements (for both TY and NTY rainy days) with the rain gauge for different wind speed~~
 143 ~~conditions (daily maximum wind speed: 0-8, 8-14, 14-18, > 18 m s⁻¹), and the results are~~
 144 ~~provided in Table 1. For the considered NTY rainy days, the daily maximum wind speeds were~~
 145 ~~less than 14 m s⁻¹, however, there were TY rainy days with wind speed > 18 m/s. A good~~
 146 ~~agreement between JWD and rain gauge measurements for both TY and NTY days (Fig.2 and~~
 147 ~~Table 1) provided the trustworthiness of the JWD data for further analysis.~~

Formatted: Font: (Default) Times New Roman, 12 pt

148
 149 The rain/RSD parameters like raindrop concentration $N(D)$ (mm⁻¹ m⁻³), radar reflectivity
 150 factor Z (mm⁶ m⁻³), liquid water content W (g m⁻³), rainfall rate R (mm h⁻¹), total number
 151 concentration N_t (m⁻³), normalized intercept parameter, N_w (m⁻³ mm⁻¹), shape parameter μ (-),
 152 slope parameter λ (mm⁻¹), and mass-weighted mean diameter D_m (mm) are estimated from the
 153 JWD measurements. The formulations for these rain/RSD parameters are detailed in Seela et al.
 154 (2017);Seela et al. (2018);Tokay et al. (2001);Bringi et al. (2003);Tokay and Short (1996). In
 155 addition to rain parameters, the rainfall kinetic energy (KE), which can be expressed in KE flux
 156 (KE_{time} , in J m⁻² h⁻¹) and KE content (KE_{mm} , J m⁻² mm⁻¹) were computed for TY and NTY
 157 rainfall using the procedures of Fornis et al. (2005);Salles et al. (2002);van Dijk et al. (2002).

Field Code Changed

Field Code Changed

158
 159 In addition to disdrometer data, remote-sensing (TRMM and MODIS) and reanalysis
 160 (ERA-interim) data sets are used to elucidate the thermodynamical and microphysical
 161 characteristics that are accountable for the possible disparities in RSDs between TY and NTY

162 rainfall. Bright band and storm heights from TRMM satellite (2A23 data product) (Iguchi et al.,
163 2000;Kummerow et al., 2001), cloud effective radii (CER) ~~cloud effective radii~~ of liquid and ice
164 particles from MODIS satellite (MOD08_D3 data product) (Platnick et al., 2015;Remer et al.,
165 2005;Nakajima and King, 1989), water vapor, convective available potential energy (CAPE),
166 relative humidity and temperature profiles from ERA-Interim (Dee et al., 2011) are considered
167 for TY and NTY rainfall. Both remote-sensing and reanalysis data sets are interpolated to 0.125°
168 $\times 0.125^\circ$ over the disdrometer site. A brief description of these data sets can be found in Seela et
169 al. (2018);Janapati et al. (2020).

Field Code Changed

Field Code Changed

Field Code Changed

Field Code Changed

170
171 Besides remote-sensing and re-analysis data sets, the radar reflectivity profiles from
172 radars mosaic are used to reveal TY and NTY rainfall characteristics. The Z profiles were
173 obtained from the six ground-based radars, and the locations of these radars are depicted with red
174 triangles in Fig. 1. Over the JWD site, the reflectivity profiles available for the period of 2005-
175 2014 are used, and further details on Taiwan radar reflectivity mosaic can be found in Chang et
176 al. (2020).

Formatted: Font: (Default) Times New Roman, 12 pt

Field Code Changed

178 3. Observational Results

179 The quality controlled JWD data showed 23074 and 20368 minutes of RSD samples,
180 respectively, for TY and NTY rainfall, and the mean raindrops concentrations of these two
181 weather ~~systems-conditions~~ are depicted in Fig. 2. In this work, raindrops of diameter greater
182 than 3 mm, 1–3 mm, and less than 1 mm are named, respectively, as large, mid, and small drops
183 (Tokay et al., 2008;Seela et al., 2018). As illustrated in Fig. 3a, perceivable segregation between
184 TY and NTY rainfall RSDs can be seen with more large drops in NTY than the TY rainfall.

Field Code Changed

185 Despite of weak distinction between TY and NTY mean rain spectra for raindrops of diameter <
186 2 mm, it can be seen that the spectra variability within TY and NTY classes is smaller than the
187 differences between averaged TY and NTY spectra. Given the dependency of raindrop
188 concentration on rainfall rate, it is ~~formidable~~ difficult to interpret alterations between TY and
189 NTY rainfall RSD from Fig. 3a. Consequently, we implemented the normalization procedure
190 (Testud et al., 2001), which is independent of the shape of the observed raindrop spectra, to the
191 TY and NTY RSDs. For TY and NTY rainfall, the drop diameter (D , mm) and raindrop
192 concentrations [$N(D)$, $\text{mm}^{-1} \text{m}^{-3}$] are normalized, respectively, by mass-weighted mean diameter
193 (D_m , mm) and normalized intercept parameter (N_w , $\text{mm}^{-1} \text{m}^{-3}$), and these normalized RSDs are
194 illustrated in Fig. 3b. A remarkable departure in the normalized RSDs spectra between NTY and
195 TY rainfall (for $D/D_m > 2$) insinuates that divergent microphysical processes were involved in
196 these two ~~weather conditions~~ weather systems.

Field Code Changed

197
198 For TY and NTY rainfall, the probability density functions (PDFs) are evaluated for D_m
199 (mass-weighted mean diameter in mm), $\log_{10}N_w$ (N_w is normalized intercept parameter in
200 $\text{mm}^{-1} \text{m}^{-3}$), $\log_{10}R$ (R is rainfall rate in mm h^{-1}), and $\log_{10}W$ (W is the liquid water content in
201 g m^{-3}) and are depicted in Fig. 4. Fig. 4a demonstrates the PDF of D_m in NTY rainfall has
202 higher distribution than TY rainfall for $D_m > 1.7$ mm. The $\log_{10}N_w$ ($\log_{10}R$) PDF distribution
203 shows peak values around 3.7 (0.3) and 3.4 (0), respectively, for TY and NTY rainfall (Fig.
204 4b). The PDF of $\log_{10}W$ shows a higher percentage at lower $\log_{10}W$ values ($\log_{10}W < -1$) in
205 NTY rainfall, and a higher percentage at higher $\log_{10}W$ values ($\log_{10}W > -1$) in TY rainfall
206 (Fig. 4d). ~~Further, a statistical (Student's t test) test executed for these four parameters (D_m ,
207 $\log_{10}N_w$, $\log_{10}R$, and $\log_{10}W$) features the rejection of the null hypothesis at 0.05 and 0.01~~

~~significance levels.~~ Further, a statistical Student's t-test (used to determine whether two data sets are significantly different from each other or not), is executed between TY and NTY rainfall D_m values. The test results rejected the null hypothesis at 0.05 and 0.01 significance levels, which confirm that the D_m values in TY rainfall are different from that of the NTY rainfall. Similarly, the Student's t-test performed for other three parameters ($\log_{10}N_w$, $\log_{10}R$, and $\log_{10}W$) also showed that these parameters in TY rainfall are different from that of the NTY rainfall.

3.1 Contribution of raindrop diameters to N_t and R

The contributions of raindrop diameter classes (diameter < 1 mm, 1–2 mm, 2–3 mm, 3–4 mm, and 4–5 mm) to N_t (m^{-3}) and R (mm h^{-1}) for TY and NTY rainfall are shown in Fig. 5. As can be seen in Fig.5a & b, for both TY and NTY rainfall, with the increase of drop diameter classes, contribution to total number concentration decreases, while that of rainfall rate increases and then lessens, and such peculiarities were noticed by previous researchers on tropical cyclones (Chen et al., 2019) and summer season rainfall (Wu et al., 2019). For both TY and NTY rainfall, small size drops (< 1 mm) grant to large number concentration (> 70%) and about 10% to rainfall rate. For both TY and NTY rainfall, raindrops with diameter 1–2 mm afford around 20% to number concentration; nonetheless, these raindrops (1–2 mm) yield around 60% (55%) to rainfall rate for TY (NTY) rainfall. The contribution of raindrops with diameters 2–3 mm to number concentration is negligible, and the rainfall rate is above 20% for both TY and NTY rainfall. Fig. 5a&b emphasize the predominant contribution of small (< 1 mm) and mid-size drops (1–3 mm) to total number concentration and rainfall rate than large drops. The

Field Code Changed

Field Code Changed

occurrence percentages of N_t (m^{-3}) ($[(N_t)_{\text{TY}} \text{ or } (N_t)_{\text{NTY}} / ((N_t)_{\text{TY}} + (N_t)_{\text{NTY}})] \times 100$) and R (mm h^{-1}) ($[(R)_{\text{TY}} \text{ or } (R)_{\text{NTY}} / ((R)_{\text{TY}} + (R)_{\text{NTY}})] \times 100$) at different diameter classes are illustrated, respectively, in Fig.5c and Fig.5d. For the first three drop diameter classes (< 1 mm, 1–2 mm, 2–3 mm), the N_t (m^{-3}) percentages are predominant in TY than NTY rainfall, and in contrast, for large drops (> 3 mm), the N_t (m^{-3}) percentages are higher in NTY than TY rainfall. Similar to the N_t (m^{-3}), the rainfall rate percentages are higher in TY than NTY rainfall for small and mid-size drops, and an opposite feature can be seen for large drops (> 3 mm).

238

239 3.2 Segregation of RSDs based on rainfall rates

To further explore the discrepancies between TY and NTY rainfall RSDs, we segregate the TY and NTY RSDs into seven rainfall rate classes (as given in ~~Table 1~~ Table 2) using the below-mentioned grouping criteria. The data points in each rainfall rate category should be sufficiently large in TY and NTY rainfall, and for each category, the mean values of rainfall rates should be nearly equal between these two weather systems conditions-(TY and NTY rainfall) (Jayalakshmi and Reddy, 2014;Deo and Walsh, 2016;Seela et al., 2017). Statistical values of these seven rainfall rate categories are specified in ~~Table 1~~ Table 2 for TY and NTY rainfall. As depicted in the table, the mean values of rainfall rates are nearly equal between these two weather systems conditions-(TY and NTY). Excluding fourth and fifth rainfall rate class (C4 and C5), the skewness values are excessive in NTY than TY rainfall. Correspondingly, these two weather systems conditions-(TY and NTY) show positive skewness designating that the rainfall rates are focused on the left to the mean. The RSDs peculiarities between TY and NTY rainfall are evaluated in percentage parameter (Ratio of $N(D)$ in TY or NTY rainfall for the raindrop

Field Code Changed

253 diameter D and rainfall rate class R to the raindrop concentration accumulations in TY and NTY
 254 rainfall) context, as explicated in Seela et al. (2018).

Field Code Changed

255 The percentage parameter of $N(D)$ for different rain rate class, $\delta(D, R) = \delta(D, R_{ck})_{TY/NTY}$
 256 is given as

$$257 \delta(D, R_{ck})_{TY} = \frac{[N(D)_{TY}]_{ck}}{([N(D)_{TY}]_{ck} + [N(D)_{NTY}]_{ck})} \times 100 \text{ -----(1)}$$

258

$$259 \delta(D, R_{ck})_{NTY} = \frac{[N(D)_{NTY}]_{ck}}{([N(D)_{TY}]_{ck} + [N(D)_{NTY}]_{ck})} \times 100 \text{ -----(2)}$$

260 Where $[N(D)_{TY}]_{ck}$ or $[N(D)_{NTY}]_{ck}$ represents the mean $N(D)$ of TY or NTY rainfall for the rain
 261 rate class “Ck”, with k=1, 2, 3, 4, 5, 6, 7 (C1: $0.1 < R < 1$, C2: $1 < R < 2$, C3: $2 < R < 5$, C4: $5 <$
 262 $R < 10$, C5: $10 < R < 30$, C6: $30 < R < 50$, and C7: $R > 50$, where R is in mm h^{-1} ; please refer to
 263 table 2).

264

265 The raindrop concentration percentages are appraised for both TY and NTY rainfall and
 266 are illustrated in Fig. 6. The percentage contribution of $N(D)$ for TY and NTY rainfall
 267 corroborated that small and mid-size drops ($< 3 \text{ mm}$) display superior percentage in TY than
 268 NTY rainfall. Nevertheless, large drops ($> 3 \text{ mm}$) unveil a higher percentage of $N(D)$ in NTY
 269 than TY rainfall.

270

271 Distributions of D_m (mm) and $\log_{10} N_w$ ($\text{m}^{-3} \text{ mm}^{-1}$) for seven rainfall rate classes are
 272 depicted with box plots in Fig. 7. As can be seen from Fig. 7a, with the increase in rainfall rate
 273 class, D_m values increase for both TY and NTY rainfall, which is due to a raise in large size
 274 drops concentration and a reduction in small drops concentration (Rosenfeld and Ulbrich,
 275 2003; Krishna et al., 2016), and similar finding were noticed by previous researchers for both

Field Code Changed

276 tropical cyclones and non-tropical cyclones rainfall (Bao et al., 2020;Deo and Walsh,
 277 2016;Jayalakshmi and Reddy, 2014;Radhakrishna and Narayana Rao, 2010). On the other hand,
 278 D_m values are greater in NTY than TY rainfall in all rainfall rate classes due to the predominant
 279 concentration of mid-size and small size raindrops in TY than NTY days (Fig.6). Compared to
 280 D_m , for all seven rainfall rate classes, the $\log_{10}N_w$ values are higher in TY than NTY rainfall
 281 (Fig.7b).

282
 283 Scatter plots for D_o [$D_o = (3.67 + \mu)/A$] and $\log_{10}N_w$ values in different rainfall rate classes
 284 (< 5 , $5-10$, $10-30$, $30-50$, and > 50 mm h⁻¹) are depicted in Fig.8a and Fig.8b, respectively, for
 285 TY and NTY rainfall. Likewise, the mean values of D_o and $\log_{10}N_w$ in different rainfall rate
 286 classes for TY and NTY rainfall are depicted, respectively, in Fig. 8c and Fig.8d. The stratiform
 287 and convective classification lines of Thompson et al. (2015) and Bringi et al. (2009) are
 288 designated, respectively, with horizontal black dotted line and slant solid line in Fig.8. With the
 289 enhancement in the rainfall rate class, D_o and $\log_{10}N_w$ distributions are narrowed for both TY and
 290 NTY rainfall. For rainfall rates > 10 mm h⁻¹ and < 10 mm h⁻¹, the D_o and $\log_{10}N_w$ data points are
 291 distributed, respectively, in the convective and stratiform region of Bringi et al. (2009) (Fig. 8a
 292 &b). With the rise in the rainfall rate class, the mean D_o values increase for both TY and NTY
 293 rainfall. Besides, for $R > 10$ mm h⁻¹, mean D_o and $\log_{10}N_w$ values are scattered in the convective
 294 region of Bringi et al. (2009) (Fig. 8c & d). As depicted in Fig. 8c & d, for rainfall rates > 10 mm
 295 h⁻¹, TY (NTY) rainfall mean $\log_{10}N_w$ values are scattered over (below) the rainfall classification
 296 line of Thompson et al. (2015) (Fig. 8c & d), and this exhibits that to segregate the TY and NTY
 297 rainfall to stratiform and convective type, Bringi et al. (2009) classification method is superior to
 298 Thompson et al. (2015).

Field Code Changed

Field Code Changed

Field Code Changed

Field Code Changed

Field Code Changed

Field Code Changed

Field Code Changed

Field Code Changed

299

300 3.3 RSDs in precipitation types

301 Ample literature showed distinctiveness in the RSDs with precipitation type, and
302 numerous methods were documented to segregate the precipitation into stratiform and
303 convective type (Ma et al., 2019; Jayalakshmi and Reddy, 2014; Ulbrich and Atlas, 2007). For
304 instance, Tokay and Short (1996) reported variations in convective precipitations to that of the
305 stratiform regimes. Some studies emphasized the importance to adopt precipitation specific
306 rainfall estimation relations (Ulbrich and Atlas, 2007). ~~In separating the TY and NTY rainfall~~
307 ~~into stratiform and convective type, we adopted the modified form of Bringi et al. (2003)~~
308 ~~classification method as mentioned in Ma et al. (2019). In this work, TY and NTY rainfall are~~
309 ~~segregated to convective and stratiform regimes based on the rain classification method detailed~~
310 ~~in Ma et al. (2019).~~ Distributions of mean $N(D)$ ($\text{m}^{-3} \text{mm}^{-1}$) with raindrop diameters for TY and
311 NTY rainfall are depicted in Fig. 9a. Except for the first drop size bin, higher drop
312 concentrations are noticed for convective rainfall than the stratiform rainfall. Concave shaped
313 $N(D)$ with broader distribution in convective than stratiform is due to the breakup of large drops
314 by collisions (Hu and Srivastava, 1995). The RSD characteristics demonstrated by the stratiform
315 and convective precipitations show similar features to that of the earlier studies for continental
316 (Jayalakshmi and Reddy, 2014) and oceanic regions (Krishna et al., 2016). On the other hand, in
317 stratiform and convective regimes, the mid-size and large drops concentration is higher in NTY
318 than TY rainfall. Variations in D_m and $\log_{10}N_w$ for both precipitations of TY and NTY are
319 depicted in Fig. 9b. The maritime and continental convective clusters of Bringi et al. (2003) are
320 depicted with gray rectangles. For both TY and NTY rainfall, larger mean D_m and $\log_{10}N_w$ values

Field Code Changed

Field Code Changed

Field Code Changed

Field Code Changed

Field Code Changed

Field Code Changed

Formatted: Check spelling and grammar

Field Code Changed

Field Code Changed

Formatted: Check spelling and grammar

Field Code Changed

Formatted: Check spelling and grammar

Field Code Changed

321 are noticed for convective precipitation. In contrast to that, in stratiform and convective regimes,
322 the NTY rainfall exhibit smaller $\log_{10}N_w$ and larger D_m values than TY rainfall.

323

324 3.4 Rainfall estimation relations

325 Uncertainties in the estimation of rainfall from weather radars can be minimized through
326 region, weather system, and precipitation specific radar reflectivity and rainfall rate ($Z-R$)
327 relations. In $Z = A R^b$ relation, size of the raindrops can be inferred from the coefficient 'A', and
328 the exponent 'b' represents microphysical process (Atlas et al., 1999;Steiner et al., 2004;Atlas
329 and Williams, 2003). The TY and NTY rainfall $Z-R$ relations are derived from the linear
330 regression applied to $10*\log_{10}R$, and Z , and are provided in Fig. 10. The coefficient values of
331 $Z-R$ relations are larger in NTY than the TY for stratiform and convective precipitations, as well
332 as for total rainfall. This variation ~~due to the presence is due the presence~~ of significant number
333 of large size drops in NTY to that of the TY rainfall. The current TY rainfall $Z-R$ relations show
334 disparity with the other locations tropical cyclones rainfall relations (Bao et al., 2020;Wen et al.,
335 2018;Janapati et al., 2020). The possible reasons for the variations in other locations' tropical
336 cyclones $Z-R$ relations to that of the present TY rainfall could be due to geographical variations
337 or the RSD measurements from different types of disdrometers(Adirosi et al., 2018).- Moreover,
338 the obtained TY and NTY days $Z-R$ relations are found to differ from the default ($Z=300 R^{1.4}$)
339 and tropical $Z-R$ relationships ($Z=250R^{1.2}$), which suggests to adopt weather and region-specific
340 $Z-R$ relations.

341

342

343

Formatted: Check spelling and grammar

Formatted: Check spelling and grammar

Formatted: Check spelling and grammar

Field Code Changed

Field Code Changed

Formatted: Check spelling and grammar

Formatted: Check spelling and grammar

Formatted: Check spelling and grammar

Field Code Changed

Field Code Changed

3.5 The rainfall rate relationships with D_m and N_w

The normalized intercept parameter and mass-weighted mean diameter values can provide the RSD features, and these parameters were found to show uniqueness with the rainfall rate (Chen et al., 2016; Janapati et al., 2020). Distribution of D_m and $\log_{10}N_w$ with rainfall rates for both weather ~~conditionssystems~~ are portrayed in Fig. 11. As can be seen from the figure, the distributions of D_m gets narrowed with the increase in rainfall rates for both ~~weather conditionsweather systems~~, and such behaviors were reported for tropical cyclone and summer season rainfall (Kumar and Reddy, 2013; Wen et al., 2018; Chang et al., 2009; Janapati et al., 2020; Chen et al., 2019; Wu et al., 2019). No further fluctuations in the D_m values at higher rainfall rates ($> 25 \text{ mm h}^{-1}$) are due to the equilibrium condition in the RSDs (attained through raindrop breakup and coalescence processes) (Hu and Srivastava, 1995), and further increase in rainfall rates is due to the increase in number concentration under RSDs equilibrium condition (Bringi and Chandrasekar, 2001). The power-law equations for D_m-R and $\log_{10}N_w-R$ are computed using a non-linear least squares method and are exemplified in Fig. 11. The evaluated D_m-R ($\log_{10}N_w-R$) relations exhibit a larger (smaller) coefficient in NTY rainfall than TY rainfall, which confirm that for given rainfall rates, the NTY rainfall had a higher D_m and lower N_w values than the TY rainfall.

3.6 $KE-R$ and $KE-D_m$ relations

The raindrops reaching the ground with a certain amount of kinetic energy (KE) can erode the soil from the ground surface. Hence, the raindrops KE or rainfall KE is one of the critical physical quantities in soil erosion studies (Wischmeier, 1959; Kinnell, 1981). As the rainfall KE is related to the raindrop diameter and its fall velocity, it can be evaluated through the

Formatted: Check spelling and grammar

Formatted: Check spelling and grammar

Field Code Changed

Field Code Changed

Formatted: Check spelling and grammar

Formatted: Check spelling and grammar

Formatted: Check spelling and grammar

Formatted: Check spelling and grammar

Formatted: Check spelling and grammar

Formatted: Check spelling and grammar

Field Code Changed

Formatted: Check spelling and grammar

Field Code Changed

Formatted: Check spelling and grammar

Formatted: Check spelling and grammar

Formatted: Check spelling and grammar

Field Code Changed

367 RSD information (Kinnell, 1981). The empirical relations between the rainfall KE and rainfall
 368 intensity are incorporated in assessing the rainfall erosivity factor (R-factor), one of the key
 369 parameters in soil erosion modeling studies (Renard et al., 1997; Janapati et al., 2019). To this
 370 end, we investigated the empirical relations between the rainfall KE (KE_{time} in $J\ m^{-2}\ h^{-1}$; KE_{mm} in
 371 $J\ m^{-2}\ mm^{-1}$) and rainfall rate ($mm\ h^{-1}$) using non-linear least-squares regression method for TY
 372 and NTY rainfall. The distribution plots of KE_{mm} and KE_{time} with R for TY and NTY rainfall are
 373 portrayed in Fig. 12. The KE_{time} - R empirical relations are derived by fitting the data points with
 374 power and liner methods. For both TY and NTY days, the power-law line fitted well by passing
 375 through the middle of the data points at both lower and higher rainfall rates than the linear fit line
 376 (Fig. 12a & b). The KE_{mm} and R data points are fitted with power, logarithmic, and exponential
 377 law. Among three forms of relations, the power-law fitted well with the data points for both TY
 378 and NTY days (Fig. 12c & d). Moreover, empirical relations between D_m (mm), the KE_{mm} are
 379 evaluated for both TY and NTY rainfall and are given in Fig. 13. Comparison of present KE - D_m
 380 relations with the East China seasonal rainfall KE - D_m ($KE = -2.33D_m^2 + 21.05D_m - 7.79$) relation
 381 shows that both TY and NTY relations in Taiwan are different from that of East China (Wen et
 382 al., 2019). The derived KE - D_m relations can be used to estimate the KE values from the remote-
 383 sensing radar (GPM DPR) measurements. The KE_{time} - R , KE_{mm} - R , and KE - D_m relations and their
 384 statistical values are given in ~~Table 2~~ Table 3. For both KE_{time} - R , KE_{mm} - R relations, the power-
 385 law exhibits higher CC and lower RMSE and NRMSE values, which suggest to adopt the power
 386 form equation to estimate the rainfall KE .

Field Code Changed

Formatted: Check spelling and grammar

Formatted: Check spelling and grammar

Formatted: Check spelling and grammar

Field Code Changed

Field Code Changed

Field Code Changed

390 4. Discussion

391 To apprehend propitious mechanisms responsible for the discrepancies in RSDs between
392 TY and NTY rainfall, re-analysis, remote sensing, and ground-based radar data sets are used.
393 The water vapor and CAPE values for TY and NTY days depicted with a box plot in Fig. 14
394 signify that NTY days had strong convective activity with vigorous updrafts and downdrafts than
395 TY days. Nonetheless, if we look at the storm and bright band heights (BBH) (Fig. 15), TY days
396 had relatively higher BBH than NTY days and there is no apparent alterations in storm heights
397 between TY and NTY days. Relatively higher BBH support the greater CER values for ice
398 particles in TY than NTY days (Fig. 16b). Nevertheless, there is no much difference in the liquid
399 particles CER median values between TY and NTY days (Fig.16a). The deep stratiform clouds
400 in TY days offer sufficient time for the growth of ice crystals to large size (via aggregation and
401 vapor deposition) and melt to big size drops once they cross the melting layer. Relatively higher
402 BBH in TY days allowed the RSDs to reach equilibrium through various microphysical
403 processes (collision, coalescence, and breakup) than NTY rainfall (Hu and Srivastava, 1995). In
404 contrast, intense convection (with resilient updrafts and downdrafts) in NTY days enhances
405 raindrops growth (through collision-coalescence and drop sorting processes), shoots smaller
406 drops at higher altitudes, and allows large drops to reach the surface. The vertical profiles of air
407 temperature and relative humidity for TY and NTY days evidently illustrate that NTY days were
408 drier compared to that of the TY rainy days (Fig. 17), and hence, the rate of evaporation of small
409 drops (that were produced through the collision breakup processes) in NTY days was higher than
410 TY days resulting in more large drops in NTY days.

411

Field Code Changed

Formatted: Check spelling and grammar

412 The radar reflectivity CFAD (contoured frequency-by-altitude diagrams) for (a) typhoon
 413 (TY) and (b) non-typhoon (NTY) days are portrayed in Fig. 18. The vertical sky blue (dark
 414 magenta) star line in Fig. 18a (Fig.18b) is the mean radar reflectivity profile of TY (NTY) days.
 415 The white-star dotted profile in Fig.18a & b is the mean of both TY and NTY days' reflectivity
 416 profiles. The mean reflectivity profile of TY (NTY) days is less (higher) than the mean of TY
 417 and NTY days' reflectivity profile. A higher occurrence percentage of lower Z values ($Z < 10$
 418 dBZ) in TY than NTY days can be seen at higher altitudes. In contrast to that, below the melting
 419 layer, the occurrence percentage of higher reflectivity values ($Z > 40$ dBZ) is higher in NTY than
 420 TY days. The mean vertical profiles of radar reflectivity for TY and NTY days are plotted in Fig.
 421 19. It can be seen from the figure that the mean reflectivity values are higher in NTY than TY
 422 days. As the radar reflectivity is directly related to the sixth power of raindrop diameter, higher
 423 reflectivity profiles in NTY than TY days infer the predominance of large drops in NTY than TY
 424 rainy days. The above-mentioned microphysical and thermodynamical processes resulted in
 425 more big size drops and few small drops in NTY than TY days, resulting in higher D_m and lower
 426 N_w values in NTY than TY days.

427

428

429

430 5. Summary and conclusions

431 Raindrop size distributions (RSDs) of typhoon (TY) and non-typhoon (NTY) rainy days
 432 have been analyzed using long-term (2004-2016) disdrometer measurements from north Taiwan.

433 Besides disdrometer data, other auxiliary data sets (remote-sensing, re-analysis, and ground-
 434 based radar) have been used to discuss the disparities in RSDs between TY and NTY

435 ~~rainfall. Along with disdrometer data, other auxiliary (remote sensing, re-analysis, and ground-~~
 436 ~~based radar) data sets have been used to elucidate the feasible mechanisms liable for the~~
 437 ~~distinctions in RSDs concerning TY and NTY rainfall.~~ The NTY days have more big size drops
 438 and less small size drops than TY days, resulting in larger D_m and smaller N_w values in NTY
 439 days. ~~Likelihood for the diverse microphysical processes between TY and NTY rainfall is~~
 440 ~~exemplified by exclusive separation in TY and NTY rainfall normalized raindrop spectra at~~
 441 ~~$D/D_m \rightarrow 2$. The mean normalized RSD of NTY precipitation has a higher occurrence of larger~~
 442 ~~drops (at $D/D_m > 2$) than TY precipitation, which indicates the possibility for diverse~~
 443 ~~microphysical processes between these two weather conditions.~~ The classification of RSDs to
 444 varying rainfall rates and precipitation (stratiform and convective) regimes clearly show smaller
 445 D_m and larger N_w values in TY than NTY days. The percentage contribution of large (small and
 446 mid-size) drops to N_t and R is lower (higher) in TY than NTY rainfall. For both TY and NTY
 447 rainy days, stratiform precipitations D_m and N_w values are smaller than the maritime and
 448 continental clusters, while, convective precipitations D_m values are approximately within the
 449 range of maritime clusters. The rainfall kinetic energy and intensity ($KE_{time}-R$ and $KE_{mm}-R$)
 450 relations evaluated for both TY and NTY rainy days reveal greater performance of power
 451 relation than other types, and confirms to use power form of $KE-R$ relations in assessing the
 452 rainfall erosivity factor for TY and NTY rainfall events. The enumerated $Z-R$, D_m-R , N_w-R ,
 453 $KE_{time}-R$, $KE_{mm}-R$, and $KE_{mm}-D_m$ relations showed profound diversity between TY and NTY
 454 rainfall and substantiate the significance of adopting precipitation specific empirical relations in
 455 evaluating the rainfall rate and kinetic energy values. Overall, present study confirms that
 456 relatively higher convective activity with drier conditions in NTY than TY days significantly
 457 wedged the disparities in RSDs with dissimilar microphysical processes. The current

458 observational outcomes could benefit in appraising the radar precipitation estimation algorithms,
459 cloud modeling, and rainfall erosivity in north Taiwan for TY and NTY rainfall events.

460

461 *Data availability.* The Era-interim re-analysis data can be obtained from
462 <https://www.ecmwf.int/en/forecasts/datasets/reanalysis-datasets/era-interim>. The TRMM data
463 can be retrieved from <https://gpm.nasa.gov/data/directory>. The MODIS cloud data product can
464 be accessed through <https://modis.gsfc.nasa.gov/data/dataproduct/mod06.php>. The ground-based
465 radar and disdrometer data are available from the corresponding author upon reasonable request.

Formatted: Default Paragraph Font, Font: (Default) +Body (Calibri), 11 pt

Formatted: Default Paragraph Font, Font: (Default) +Body (Calibri), 11 pt

Formatted: Default Paragraph Font, Font: (Default) +Body (Calibri), 11 pt

466

467 *Author contributions.* JJ and BKS conceptualized the idea; PLL and EJ provided funding
468 acquisition, project administration, and observation data; JJ, BKS, and MTL conducted the
469 detailed analysis; PLL, and EJ supervised the analysis; JJ, BKS wrote the initial manuscript; JJ,
470 BKS, PLL reviewed and revised the manuscript; all authors involved in writing the manuscript
471 and revisions.

472

473 *Competing interests.* No conflict of interest is declared by the all authors.

474

475 *Acknowledgements.* We acknowledge the Central Weather Bureau (CWB) of Taiwan, in
476 facilitating the radar reflectivity data, and Tropical Rainfall Measuring Mission (TRMM), ERA-
477 Interim and MODIS research team for their efforts in providing the data. This research work is
478 carried out under the Taiwan Ministry of Science and Technology (MOST) grant numbers:
479 MOST 108-2111-M-008-028, MOST 108-2625-M-008-011, MOST: 104-2923-M-008-003 and
480 partially by “Earthquake-Disaster & Risk Evaluation and Management Center, E-DREaM” from

481 The Featured Areas Research Center Program within the framework of the Higher Education
482 Sprout Project by the Ministry of Education (MOE), Taiwan. The first author, JJ is supported by
483 the grant number MOST 108-2811-M-008-558, and second author, BKS, by MOST 108-2625-
484 M-008-011 and MOST 108-2811-M-008-595.

485 References

486

487 Atlas, D., Ulbrich, C. W., Marks Jr, F. D., Amitai, E., and Williams, C. R.: Systematic variation
488 of drop size and radar-rainfall relations, *Journal of Geophysical Research: Atmospheres*,
489 104, 6155-6169, 10.1029/1998JD200098, 1999.

490 Atlas, D., and Williams, C. R.: The Anatomy of a Continental Tropical Convective Storm,
491 *Journal of the Atmospheric Sciences*, 60, 3-15, 10.1175/1520-
492 0469(2003)060<0003:Taoact>2.0.Co;2, 2003.

493 Bao, X., Wu, L., Zhang, S., Li, Q., Lin, L., Zhao, B., Wu, D., Xia, W., and Xu, B.: Distinct
494 Raindrop Size Distributions of Convective Inner- and Outer-Rainband Rain in Typhoon
495 Maria (2018), *Journal of Geophysical Research: Atmospheres*, 125, e2020JD032482,
496 10.1029/2020jd032482, 2020.

497 Bringi, V., Williams, C., Thurai, M., and May, P.: Using dual-polarized radar and dual-frequency
498 profiler for DSD characterization: A case study from Darwin, Australia, *Journal of*
499 *Atmospheric and Oceanic Technology*, 26, 2107-2122, 2009.

500 Bringi, V. N., and Chandrasekar, V.: *Polarimetric Doppler Weather Radar: Principles and*
501 *Applications*, Cambridge University Press., 2001.

502 Bringi, V. N., Chandrasekar, V., Hubbert, J., Gorgucci, E., Randeu, W. L., and Schoenhuber, M.:
503 Raindrop Size Distribution in Different Climatic Regimes from Disdrometer and Dual-
504 Polarized Radar Analysis, *Journal of the Atmospheric Sciences*, 60, 354-365,
505 10.1175/1520-0469(2003)060<0354:RSDIDC>2.0.CO;2, 2003.

Formatted: Do not check spelling or grammar

Formatted: Justified, Indent: Left: 0 cm, Hanging: 1 cm, Line spacing: Double

506 Chang, J. M., Chen, H. E., Jou, B. J. D., Tsou, N. C., and Lin, G. W.: Characteristics of Rainfall
507 Intensity, Duration, and Kinetic Energy for Landslide Triggering in Taiwan, Engineering
508 Geology, 231, 81-87, 10.1016/j.enggeo.2017.10.006, 2017.

509 Chang, P.-L., Zhang, J., Tang, Y.-S., Tang, L., Lin, P.-F., Langston, C., Kaney, B., Chen, C.-R.,
510 and Howard, K.: An Operational Multi-Radar Multi-Sensor QPE System in Taiwan,
511 Bulletin of the American Meteorological Society, 1-56, 10.1175/bams-d-20-0043.1, 2020.

512 Chang, W.-Y., Wang, T.-C. C., and Lin, P.-L.: Characteristics of the Raindrop Size Distribution
513 and Drop Shape Relation in Typhoon Systems in the Western Pacific from the 2D Video
514 Disdrometer and NCU C-Band Polarimetric Radar, Journal of Atmospheric and Oceanic
515 Technology, 26, 1973-1993, 10.1175/2009jtecha1236.1, 2009.

516 Chen, B., Wang, J., and Gong, D.: Raindrop size distribution in a midlatitude continental squall
517 line measured by thies optical disdrometers over East China, J. Appl. Meteor. Climatol.,
518 55, 621–634, 10.1175/JAMC-D-15-0127.1, 2016.

519 Chen, C.-S., and Chen, Y.-L.: The Rainfall Characteristics of Taiwan, Monthly Weather Review,
520 131, 1323-1341, 10.1175/1520-0493(2003)131<1323:TRCOT>2.0.CO;2, 2003.

521 Chen, C.-S., Chen, Y.-L., Liu, C.-L., Lin, P.-L., and Chen, W.-C.: Statistics of Heavy Rainfall
522 Occurrences in Taiwan, Weather and Forecasting, 22, 981-1002, 10.1175/waf1033.1, 2007.

523 Chen, G., Zhao, K., Zhang, G., Huang, H., Liu, S., Wen, L., Yang, Z., Yang, Z., Xu, L., and Zhu,
524 W.: Improving Polarimetric C-Band Radar Rainfall Estimation with Two-Dimensional
525 Video Disdrometer Observations in Eastern China, Journal of Hydrometeorology, 18,
526 1375-1391, 10.1175/jhm-d-16-0215.1, 2017.

527 Chen, J.-M., Li, T., and Shih, C.-F.: Tropical Cyclone– and Monsoon-Induced Rainfall
528 Variability in Taiwan, Journal of Climate, 23, 4107-4120, 10.1175/2010jcli3355.1, 2010.

529 Chen, J.-M., and Chen, H.-S.: Interdecadal Variability of Summer Rainfall in Taiwan Associated
530 with Tropical Cyclones and Monsoon, *Journal of Climate*, 24, 5786-5798,
531 10.1175/2011jcli4043.1, 2011.

532 Chen, K., Chu, C.-Y., and Tzeng, Y.-C.: A semi-empirical model of rain attenuation at Ka-band
533 in Northern Taiwan, *Progress In Electromagnetics Research*, 16, 213-223, 2011.

534 Chen, T.-C., Yen, M.-C., Hsieh, J.-C., and Arritt, R. W.: Diurnal and Seasonal Variations of the
535 Rainfall Measured by the Automatic Rainfall and Meteorological Telemetry System in
536 Taiwan, *Bulletin of the American Meteorological Society*, 80, 2299-2312, 10.1175/1520-
537 0477(1999)080<2299:DASVOT>2.0.CO;2, 1999.

538 Chen, Y., Duan, J., An, J., and Liu, H.: Raindrop Size Distribution Characteristics for Tropical
539 Cyclones and Meiyu-Baiu Fronts Impacting Tokyo, Japan, *Atmosphere-Basel*, 10, 391,
540 2019.

541 Chu, P.-S., Zhao, X., Lee, C.-T., and Lu, M.-M.: Climate prediction of tropical cyclone activity
542 in the vicinity of Taiwan using the multivariate least absolute deviation regression method,
543 *Terrestrial Atmospheric and Oceanic Sciences*, 18, 805, 2007.

544 Chu, Y.-H., and Su, C.-L.: An Investigation of the Slope–Shape Relation for Gamma Raindrop
545 Size Distribution, *Journal of Applied Meteorology and Climatology*, 47, 2531-2544,
546 10.1175/2008jamc1755.1, 2008.

547 Dee, D. P., Uppala, S., Simmons, A., Berrisford, P., Poli, P., Kobayashi, S., Andrae, U.,
548 Balmaseda, M., Balsamo, G., and Bauer, d. P.: The ERA-Interim Reanalysis:
549 Configuration and Performance of the Data Assimilation System, *Quarterly Journal of the*
550 *royal meteorological society*, 137, 553-597, 2011.

551 Deo, A., and Walsh, K. J.: Contrasting tropical cyclone and non-tropical cyclone related rainfall
552 drop size distribution at Darwin, Australia, *Atmospheric Research*, 181, 81-94, 2016.

553 Fornis, R. L., Vermeulen, H. R., and Nieuwenhuis, J. D.: Kinetic Energy–Rainfall Intensity
554 Relationship For Central Cebu, Philippines for Soil Erosion Studies, *Journal of*
555 *Hydrology*, 300, 20-32, 10.1016/j.jhydrol.2004.04.027, 2005.

556 Hu, Z., and Srivastava, R. C.: Evolution of Raindrop Size Distribution by Coalescence, Breakup,
557 and Evaporation: Theory and Observations, *Journal of the Atmospheric Sciences*, 52,
558 1761-1783, 10.1175/1520-0469(1995)052<1761:EORSDB>2.0.CO;2, 1995.

559 Iguchi, T., Kozu, T., Meneghini, R., Awaka, J., and Okamoto, K. i.: Rain-Profiling Algorithm for
560 the TRMM Precipitation Radar, *Journal of Applied Meteorology*, 39, 2038-2052,
561 10.1175/1520-0450(2001)040<2038:RPAFTT>2.0.CO;2, 2000.

562 Janapati, J., Reddy, V., Reddy, K., Lin, P.-L., and Liu, C.-Y.: A study on raindrop size
563 distribution variability in before and after landfall precipitations of tropical cyclones
564 observed over southern India, *Journal of Atmospheric and Solar-Terrestrial Physics*, 159,
565 23-40, 2017.

566 Janapati, J., Seela, B. K., Lin, P.-L., Wang, P. K., and Kumar, U.: An assessment of tropical
567 cyclones rainfall erosivity for taiwan, *Scientific reports*, 9, 15862, 2019.

568 Janapati, J., Seela, B. K., Lin, P.-L., Wang, P. K., Tseng, C.-H., Reddy, K. K., Hashiguchi, H.,
569 Feng, L., Das, S. K., and Unnikrishnan, C. K.: Raindrop Size Distribution Characteristics
570 of Indian and Pacific Ocean Tropical Cyclones Observed at India and Taiwan Sites,
571 *Journal of the Meteorological Society of Japan. Ser. II*, 98, 299-317, 10.2151/jmsj.2020-
572 015, 2020.

573 Jayalakshmi, J., and Reddy, K. K.: Raindrop size distributions of southwest and northeast
 574 monsoon heavy precipitation observed over Kadapa (14°4'N, 78°82'E), a semi-arid region
 575 of India, *Current Science*, 107, 1312-1320, 2014.

576 Joss, J., and Waldvogel, A.: Raindrop Size Distribution and Sampling Size Errors, *Journal of the*
 577 *Atmospheric Sciences*, 26, 566-569, 10.1175/1520-
 578 0469(1969)026<0566:RSDASS>2.0.CO;2, 1969.

579 Jung, S.-A., Lee, D.-I., Jou, B. J.-D., and Uyeda, H.: Microphysical Properties of Maritime
 580 Squall Line Observed on June 2, 2008 in Taiwan, *Journal of the Meteorological Society of*
 581 *Japan. Ser. II*, 90, 833-850, 10.2151/jmsj.2012-516, 2012.

582 Kinnell, P. I. A.: Rainfall Intensity-Kinetic Energy Relationships for Soil Loss Prediction1, *Soil*
 583 *Science Society of America Journal*, 45, 153-155,
 584 10.2136/sssaj1981.03615995004500010033x, 1981.

585 Krishna, U. V. M., Reddy, K. K., Seela, B. K., Shirooma, R., Lin, P.-L., and Pan, C.-J.: Raindrop
 586 size distribution of easterly and westerly monsoon precipitation observed over Palau
 587 islands in the Western Pacific Ocean, *Atmospheric Research*, 174-175, 41-51,
 588 <https://doi.org/10.1016/j.atmosres.2016.01.013>, 2016.

589 Kumar, S. B., and Reddy, K. K.: Rain drop size distribution characteristics of cyclonic and north
 590 east monsoon thunderstorm precipitating clouds observed over Kadapa (14.47°N,
 591 78.82°E), tropical semi-arid region of India, *Mausam*, 64, 35–48, 2013.

592 Kumari, N., Kumar, S. B., Jayalakshmi, J., and Reddy, K. K.: Raindrop size distribution
 593 variations in JAL and NILAM cyclones induced precipitation observed over Kadapa
 594 (14.47 o N, 78.82 o E), a tropical semi-arid region of India, *Indian Journal of Radio and*
 595 *Space Physics*, 43, 57–66, 2014.

596 Kummerow, C., Hong, Y., Olson, W. S., Yang, S., Adler, R. F., McCollum, J., Ferraro, R., Petty,
597 G., Shin, D. B., and Wilheit, T. T.: The Evolution of the Goddard Profiling Algorithm
598 (GPROF) for Rainfall Estimation from Passive Microwave Sensors, *Journal of Applied*
599 *Meteorology*, 40, 1801-1820, 10.1175/1520-0450(2001)040<1801:TEOTGP>2.0.CO;2,
600 2001.

601 Lee, G. W., and Zawadzki, I.: Variability of Drop Size Distributions: Noise and Noise Filtering
602 in Disdrometric Data, *Journal of Applied Meteorology*, 44, 634-652, 10.1175/JAM2222.1,
603 2005.

604 Lee, M.-T., Lin, P.-L., Chang, W.-Y., Seela, B. K., and Janapati, J.: Microphysical
605 Characteristics and Types of Precipitation for Different Seasons over North Taiwan,
606 *Journal of the Meteorological Society of Japan. Ser. II*, 97, 841-865, 10.2151/jmsj.2019-
607 048, 2019.

608 Liang, A., Oey, L., Huang, S., and Chou, S.: Long-term trends of typhoon-induced rainfall over
609 Taiwan: In situ evidence of poleward shift of typhoons in western North Pacific in recent
610 decades, *Journal of Geophysical Research: Atmospheres*, 122, 2750-2765,
611 10.1002/2017jd026446, 2017.

612 Liao, L., Meneghini, R., and Tokay, A.: Uncertainties of GPM DPR Rain Estimates Caused by
613 DSD Parameterizations, *Journal of Applied Meteorology and Climatology*, 53, 2524-2537,
614 10.1175/JAMC-D-14-0003.1, 2014.

615 Lin, G.-W., and Chen, H.: The relationship of rainfall energy with landslides and sediment
616 delivery, *Engineering geology*, 125, 108-118, 2012.

617 Lu, J.-Y., Su, C.-C., Lu, T.-F., and Maa, M.-M.: Number and volume raindrop size distributions
618 in Taiwan, *Hydrological Processes*, 22, 2148-2158, 10.1002/hyp.6814, 2008.

619 Ma, Y., Ni, G., Chandra, C. V., Tian, F., and Chen, H.: Statistical characteristics of raindrop size
620 distribution during rainy seasons in the Beijing urban area and implications for radar
621 rainfall estimation, *Hydrology and Earth System Sciences*, 23, 4153-4170, 2019.

622 Maki, M., Keenan, T. D., Sasaki, Y., and Nakamura, K.: Characteristics of the Raindrop Size
623 Distribution in Tropical Continental Squall Lines Observed in Darwin, Australia, *Journal*
624 *of Applied Meteorology*, 40, 1393-1412, 10.1175/1520-
625 0450(2001)040<1393:COTRSD>2.0.CO;2, 2001.

626 McFarquhar, G. M., and List, R.: The Effect of Curve Fits for the Disdrometer Calibration on
627 Raindrop Spectra, Rainfall Rate, and Radar Reflectivity, *Journal of Applied Meteorology*,
628 32, 774-782, 10.1175/1520-0450(1993)032<0774:TEOCFF>2.0.CO;2, 1993.

629 McFarquhar, G. M., Hsieh, T.-L., Freer, M., Mascio, J., and Jewett, B. F.: The characterization
630 of ice hydrometeor gamma size distributions as volumes in $N_0-\lambda-\mu$ phase space:
631 Implications for microphysical process modeling, *Journal of the Atmospheric Sciences*, 72,
632 892-909, 2015.

633 Nakajima, T., and King, M. D.: Determination of the Optical Thickness and Effective Particle
634 Radius of Clouds from Reflected Solar Radiation Measurements. Part I: Theory, *Journal of*
635 *the Atmospheric Sciences*, 47, 1878-1893, 10.1175/1520-
636 0469(1990)047<1878:DOTOTA>2.0.CO;2, 1989.

637 Nakamura, K., and Iguchi, T.: Dual-wavelength Radar Algorithm, in: *Measuring precipitation*
638 *from space*, Springer, 225-234, 2007.

639 Platnick, S., King, M., and Hubanks, P.: MODIS Atmosphere L3 Daily Product, NASA MODIS
640 Adaptive Processing System, Goddard Space Flight Center, in, 2015.

641 Radhakrishna, B., and Narayana Rao, T.: Differences in cyclonic raindrop size distribution from
642 southwest to northeast monsoon season and from that of noncyclonic rain, *Journal of*
643 *Geophysical Research: Atmospheres*, 115, 10.1029/2009jd013355, 2010.

644 Remer, L. A., Kaufman, Y. J., Tanré, D., Mattoo, S., Chu, D. A., Martins, J. V., Li, R. R.,
645 Ichoku, C., Levy, R. C., Kleidman, R. G., Eck, T. F., Vermote, E., and Holben, B. N.: The
646 MODIS Aerosol Algorithm, Products, and Validation, *Journal of the Atmospheric*
647 *Sciences*, 62, 947-973, 10.1175/JAS3385.1, 2005.

648 Renard, K. G., Foster, G. R., Weesies, G. A., McCool, D. K., and Yoder, D. C.: Predicting Soil
649 Erosion by Water: A Guide to Conservation Planning with the Revised Universal Soil Loss
650 Equation (RUSLE) (Agricultural Handbook 703). US Department of Agriculture,
651 Washington, DC,, 1997.

652 Rosenfeld, D., and Ulbrich, C. W.: Cloud Microphysical Properties, Processes, and Rainfall
653 Estimation Opportunities, *Meteorological Monographs*, 52, 237-258, 10.1175/0065-
654 9401(2003)030<0237:CMPPAR>2.0.CO;2, 2003.

655 Ryzhkov, A. V., and Zrnić, D. S.: Comparison of Dual-Polarization Radar Estimators of Rain,
656 *Journal of Atmospheric and Oceanic Technology*, 12, 249-256, 10.1175/1520-
657 0426(1995)012<0249:CODPRE>2.0.CO;2, 1995.

658 Salles, C., Poesen, J., and Sempere-Torres, D.: Kinetic Energy of Rain and Its Functional
659 Relationship With Intensity, *Journal of Hydrology*, 257, 256-270, 10.1016/S0022-
660 1694(01)00555-8, 2002.

661 Sauvageot, H., and Lacaux, J.-P.: The Shape of Averaged Drop Size Distributions, *Journal of the*
662 *Atmospheric Sciences*, 52, 1070-1083, 10.1175/1520-
663 0469(1995)052<1070:TSOADS>2.0.CO;2, 1995.

664 Seela, B. K., Reddy, K. K., Jayalakshmi, J., Rao, T. N., Lin, P.-L., Liu, C.-Y., and Kumar, U.:
665 Precipitation and cloud microstructure variations between two southern Indian stations,
666 Remote Sensing of the Atmosphere, Clouds, and Precipitation VI, 2016, 98761O,
667 Seela, B. K., Janapati, J., Lin, P.-L., Reddy, K. K., Shirooka, R., and Wang, P. K.: A Comparison
668 Study of Summer Season Raindrop Size Distribution Between Palau and Taiwan, Two
669 Islands in Western Pacific, Journal of Geophysical Research: Atmospheres, 122, 11,787-
670 711,805, 10.1002/2017jd026816, 2017.

671 Seela, B. K., Janapati, J., Lin, P.-L., Wang, P. K., and Lee, M.-T.: Raindrop Size Distribution
672 Characteristics of Summer and Winter Season Rainfall Over North Taiwan, Journal of
673 Geophysical Research: Atmospheres, 123, 11,602-611,624, 10.1029/2018jd028307, 2018.

674 Sheppard, B. E.: Effect of Irregularities in the Diameter Classification of Raindrops by the Joss-
675 Waldvogel Disdrometer, Journal of Atmospheric and Oceanic Technology, 7, 180-183,
676 10.1175/1520-0426(1990)007<0180:EOIITD>2.0.CO;2, 1990.

677 Sheppard, B. E., and Joe, P. I.: Comparison of Raindrop Size Distribution Measurements by a
678 Joss-Waldvogel Disdrometer, a PMS 2DG Spectrometer, and a POSS Doppler Radar,
679 Journal of Atmospheric and Oceanic Technology, 11, 874-887, 10.1175/1520-
680 0426(1994)011<0874:CORSDM>2.0.CO;2, 1994.

681 Steiner, M., Smith, J. A., and Uijlenhoet, R.: A Microphysical Interpretation of Radar
682 Reflectivity–Rain Rate Relationships, Journal of the Atmospheric Sciences, 61, 1114-1131,
683 10.1175/1520-0469(2004)061<1114:Amiorr>2.0.Co;2, 2004.

684 Testud, J., Oury, S., Black, R. A., Amayenc, P., and Dou, X.: The Concept of “Normalized”
685 Distribution to Describe Raindrop Spectra: A Tool for Cloud Physics and Cloud Remote

686 Sensing, Journal of Applied Meteorology, 40, 1118-1140, 10.1175/1520-
687 0450(2001)040<1118:TCOND>2.0.CO;2, 2001.

688 Thompson, E. J., Rutledge, S. A., Dolan, B., and Thurai, M.: Drop Size Distributions and Radar
689 Observations of Convective and Stratiform Rain over the Equatorial Indian and West
690 Pacific Oceans, Journal of the Atmospheric Sciences, 72, 4091-4125, 10.1175/JAS-D-14-
691 0206.1, 2015.

692 Tokay, A., and Short, D. A.: Evidence from Tropical Raindrop Spectra of the Origin of Rain
693 from Stratiform versus Convective Clouds, Journal of Applied Meteorology, 35, 355-371,
694 10.1175/1520-0450(1996)035<0355:Efrso>2.0.Co;2, 1996.

695 Tokay, A., Kruger, A., and Krajewski, W. F.: Comparison of Drop Size Distribution
696 Measurements by Impact and Optical Disdrometers, Journal of Applied Meteorology, 40,
697 2083-2097, 10.1175/1520-0450(2001)040<2083:CODSDM>2.0.CO;2, 2001.

698 Tokay, A., Bashor, P. G., Habib, E., and Kasparis, T.: Raindrop Size Distribution Measurements
699 in Tropical Cyclones, Monthly Weather Review, 136, 1669-1685,
700 10.1175/2007mwr2122.1, 2008.

701 Tokay, A., Petersen, W. A., Gatlin, P., and Wingo, M.: Comparison of Raindrop Size
702 Distribution Measurements by Collocated Disdrometers, Journal of Atmospheric and
703 Oceanic Technology, 30, 1672-1690, 10.1175/JTECH-D-12-00163.1, 2013.

704 Tu, J.-Y., and Chou, C.: Changes in precipitation frequency and intensity in the vicinity of
705 Taiwan: typhoon versus non-typhoon events, Environmental Research Letters, 8, 014023,
706 10.1088/1748-9326/8/1/014023, 2013.

707 Ulbrich, C. W., and Atlas, D.: Microphysics of Raindrop Size Spectra: Tropical Continental and
 708 Maritime Storms, *Journal of Applied Meteorology and Climatology*, 46, 1777-1791,
 709 10.1175/2007JAMC1649.1, 2007.
 710 van Dijk, A. I. J. M., Bruijnzeel, L. A., and Rosewell, C. J.: Rainfall Intensity–Kinetic Energy
 711 Relationships: A Critical Literature Appraisal, *Journal of Hydrology*, 261, 1-23,
 712 10.1016/S0022-1694(02)00020-3, 2002.
 713 Wen, L., Zhao, K., Chen, G., Wang, M., Zhou, B., Huang, H., Hu, D., Lee, W.-C., and Hu, H.:
 714 Drop size distribution characteristics of seven typhoons in China, *J. Geophys. Res. Atmos.*,
 715 123, 6529–6548, doi:10.1029/2017JD027950, 2018.
 716 Wen, L., Zhao, K., Wang, M., and Zhang, G.: Seasonal Variations of Observed Raindrop Size
 717 Distribution in East China, *Advances in Atmospheric Sciences*, 36, 346-362, 2019.
 718 Wischmeier, W. H.: A Rainfall Erosion Index for a Universal Soil-Loss Equation¹, *Soil Science*
 719 *Society of America Journal*, 23, 246-249, 10.2136/sssaj1959.03615995002300030027x,
 720 1959.
 721 Wu, Z., Zhang, Y., Zhang, L., Lei, H., Xie, Y., Wen, L., and Yang, J.: Characteristics of summer
 722 season raindrop size distribution in three typical regions of western Pacific, *Journal of*
 723 *Geophysical Research: Atmospheres*, 124, 4054-4073, 2019.
 724 Zhang, Y., Liu, L., Bi, S., Wu, Z., Shen, P., Ao, Z., Chen, C., and Zhang, Y.: Analysis of dual-
 725 polarimetric radar variables and quantitative precipitation estimators for landfall typhoons
 726 and squall lines based on disdrometer data in southern China, *Atmosphere*, 10, 30, 2019.
 727
 728

Table 1. The JWD and rain gauge comparison results (n: number of rainy days, CC: correlation coefficient, RMSE: root mean square error) for different wind speed conditions (daily maximum wind speed: 0-8, 8-14, 14-18, > 18 m s⁻¹). Note: there were no NTY rainy days with daily maximum wind speed > 14 m s⁻¹.

<u>Wind speed</u> <u>(m s⁻¹)</u>	<u>TY</u>			<u>NTY</u>		
	<u>n</u>	<u>CC</u>	<u>RMSE (mm)</u>	<u>n</u>	<u>CC</u>	<u>RMSE (mm)</u>
<u>0-8</u>	<u>21</u>	<u>0.989</u>	<u>6.305</u>	<u>113</u>	<u>0.956</u>	<u>3.853</u>
<u>8-14</u>	<u>27</u>	<u>0.99</u>	<u>5.153</u>	<u>18</u>	<u>0.942</u>	<u>3.482</u>
<u>14-18</u>	<u>8</u>	<u>0.953</u>	<u>18.112</u>	<u>=</u>	<u>=</u>	<u>=</u>
<u>>18</u>	<u>3</u>	<u>0.996</u>	<u>7.448</u>	<u>=</u>	<u>=</u>	<u>=</u>

Table 1 Table 2. Rainy minutes (N), mean, standard deviation (Std), Skewness and Kurtosis of seven rainfall rate classes for typhoon (TY) and non-typhoon (NTY) rainy days of summer seasons.

Rain rate class	Rain rate threshold (mm h ⁻¹)	Typhoon (TY)					non-typhoon (NTY)				
		No. of samples	Mean (mm h ⁻¹)	Standard deviation (mm h ⁻¹)	Skewness	Kurtosis	No. of samples	Mean (mm h ⁻¹)	Standard deviation (mm h ⁻¹)	Skewness	Kurtosis
C1	$0.1 \leq R < 1$	9317	0.43	0.26	0.55	2.1	10661	0.4	0.25	0.71	2.34
C2	$1 \leq R < 2$	3274	1.44	0.29	0.24	1.84	3193	1.43	0.29	0.29	1.88
C3	$2 \leq R < 5$	4747	3.29	0.85	0.31	1.92	3404	3.17	0.83	0.46	2.1
C4	$5 \leq R < 10$	2799	7	1.4	0.43	2.04	1404	6.98	1.42	0.43	2.01
C5	$10 \leq R < 30$	2313	16.44	5.24	0.77	2.59	1234	17.46	5.6	0.5	2.08
C6	$30 \leq R < 50$	393	38.31	5.73	0.37	1.92	320	37.88	5.67	0.45	2.01
C7	$R > 50$	231	67.15	14.91	1.16	3.97	152	65.86	14.94	1.51	5.18
total		23074	4.88	9.38	4.59	31.51	20368	3.59	8.38	5.2	38.9

753
754
755
756
757
758
759
760
761
762
763
764
765
766
767
768
769

Table 2 Table 3. Statistical parameters [correlation coefficient: R^2 , Root mean square error (RMSE), normalized RMSE] for typhoon (TY) and non-typhoon (NTY) rainy days.
Note: Units for RMSE are $J\ m^{-2}\ h^{-1}$ for $KE_{time}-R$ relations and $J\ m^{-2}\ mm^{-1}$ for $KE_{mm}-R$ and $KE_{mm}-D_m$ relations.

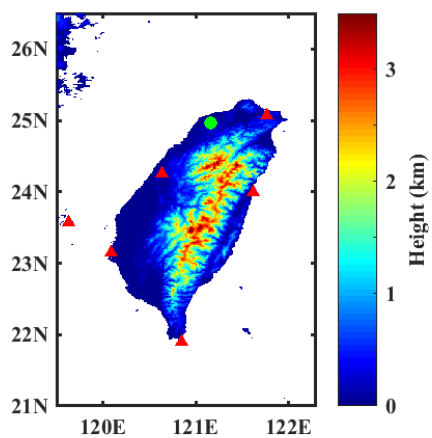
Weather condition Weather system	Statistical parameter	$KE_{time}-R$		$KE_{mm}-R$			$KE_{mm}-D_m$
		Linear	Power	Power	Exp	Log	Second order polynomial
TY	R^2	0.986	0.994	0.694	0.68	0.68	0.992
	RMSE	37.488	24.785	3.973	10.227	4.047	12.396
	NRMSE	0.306	0.202	0.032	0.083	0.033	2.514
NTY	R^2	0.984	0.99	0.646	0.639	0.639	0.988
	RMSE	38.012	30.745	4.599	11.017	4.636	12.93
	NRMSE	0.322	0.26	0.039	0.093	0.039	2.803

Formatted: Font: 12 pt
Formatted: Font: 12 pt
Formatted: Font: 12 pt
Formatted: Font: 12 pt
Formatted: Font: 12 pt
Formatted: Font: (Default) Times New Roman, 12 pt

770
771
772
773
774
775
776

777

Figures



778

779 **Figure 1.** Map of Taiwan with disdrometer (green color circle) and radars (red color triangles)

780 sites.

781

782

783

784

785

786

787

788

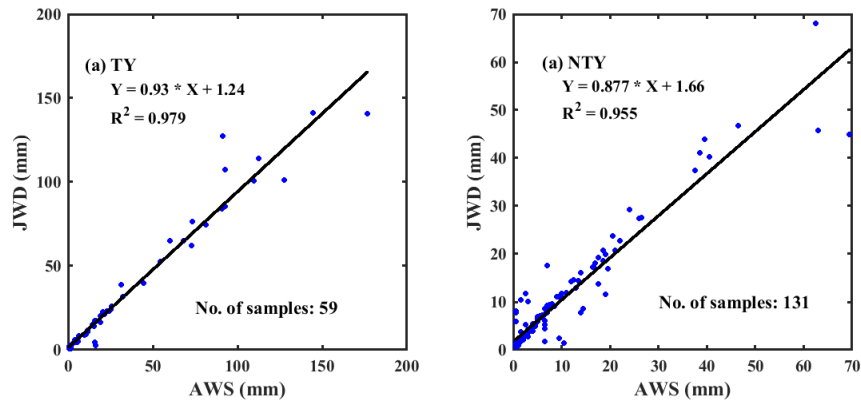
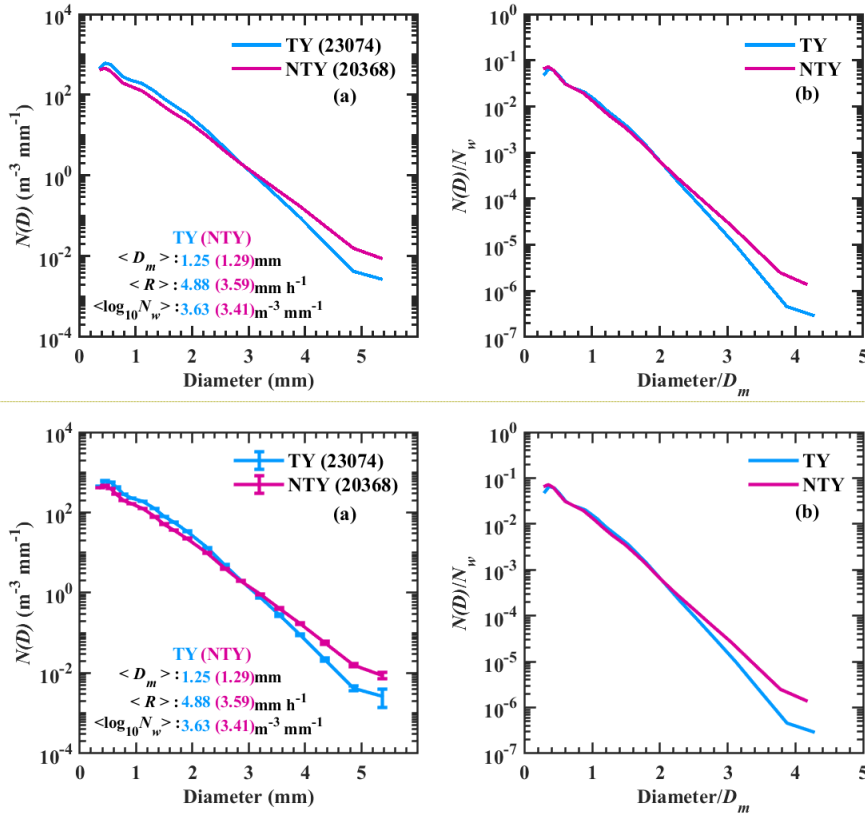


Figure 2. The JWD and rain gauge daily accumulations scatter plot for (a) typhoon (TY) and (b) non-typhoon (NTY) rainfall.



Formatted: Font: (Default) Times New Roman, 12 pt, Bold

Figure 3. (a) Distributions of mean concentration $[N(D)$, in $\text{mm}^{-1} \text{m}^{-3}]$ with raindrop diameter for typhoon (TY) and non-typhoon (NTY) rainfall and their (b) normalized spectra.

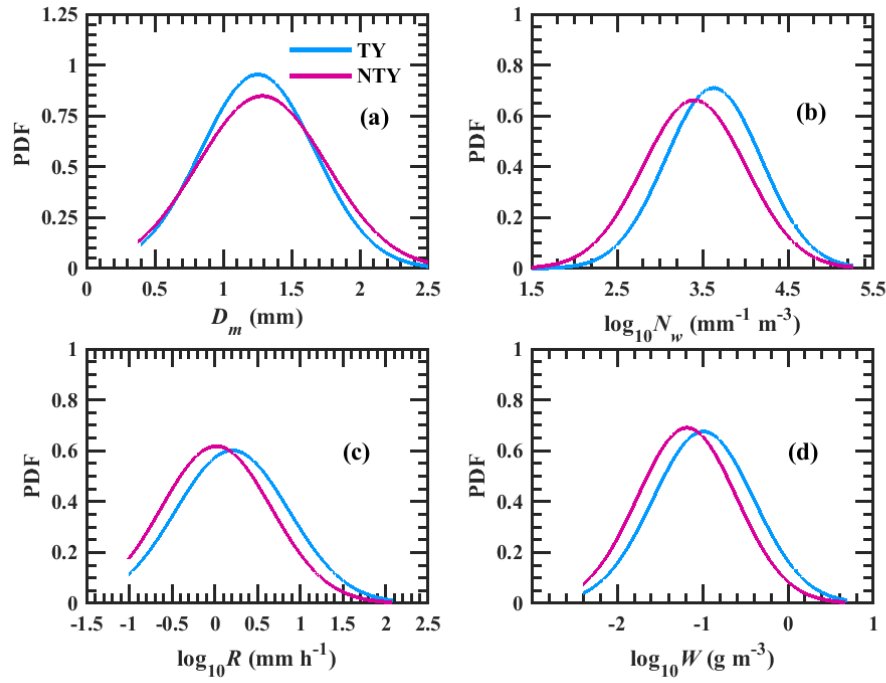
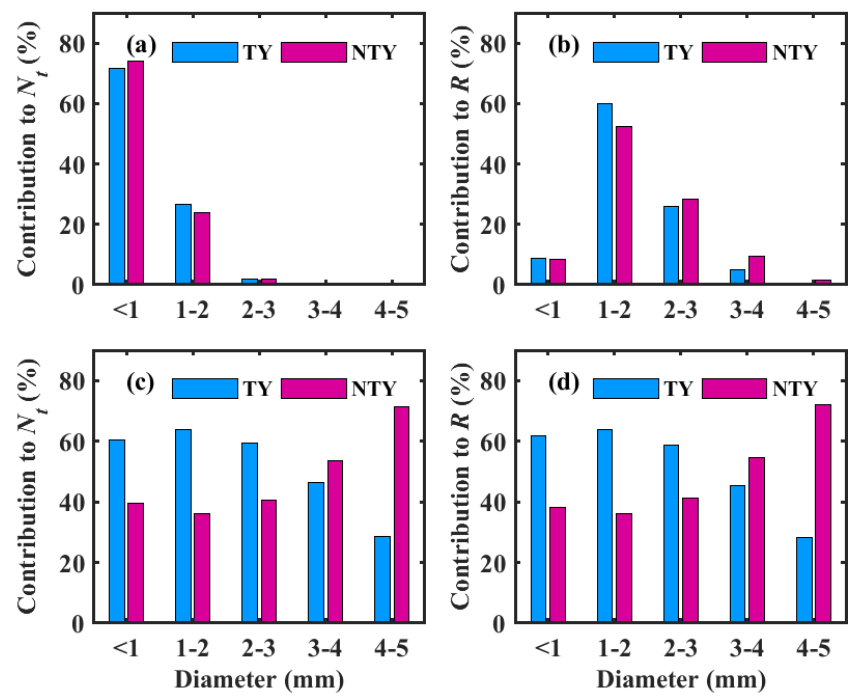


Figure 4. The probability distribution functions (PDF) of (a) mass-weighted mean diameter, D_m (mm), (b) $\log_{10} N_w$ (N_w is the normalized intercept parameter in $\text{mm}^{-1} \text{m}^{-3}$), (c) $\log_{10} R$ (R is rainfall rate in mm h^{-1}), and (d) $\log_{10} W$ (W is the liquid water content in g m^{-3}) for typhoon (TY) and non-typhoon (NTY) rainfall.



Formatted: Font: (Default) Times New Roman, 12 pt, Bold

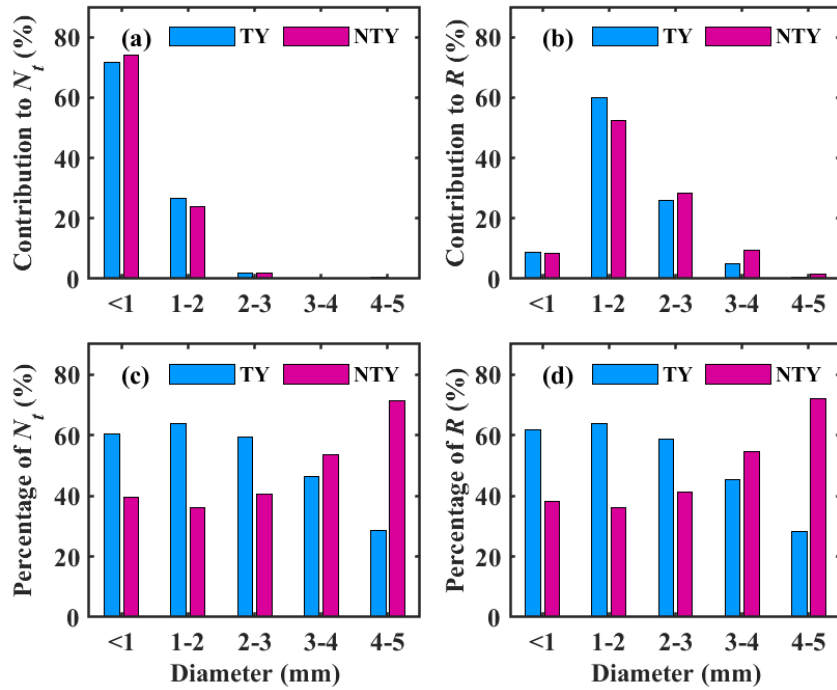


Figure 5. Contribution of drop diameter classes (Diameter < 1 mm, 1–2 mm, 2–3 mm, 3–4 mm, and 4–5 mm) to (a) total number concentration N_t (m^{-3}) and (b) rainfall rate R (mm h^{-1}) in typhoon (TY) and non-typhoon (NTY) rainfall. [Occurrence percentage of Percentage of](#) (c) total number concentration N_t (m^{-3}) and (d) rainfall rate R (mm h^{-1}) in each diameter class for typhoon (TY) and non-typhoon (NTY) rainfall.

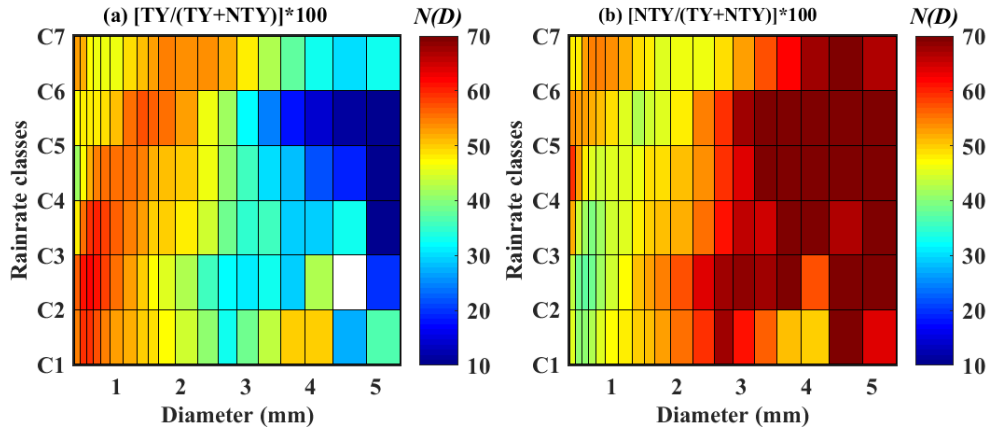


Figure 6 Percentage contribution of $N(D)$ ($\text{mm}^{-1} \text{m}^{-3}$) in different rainfall rate classes for typhoon (TY) and non-typhoon (NTY) rainfall.

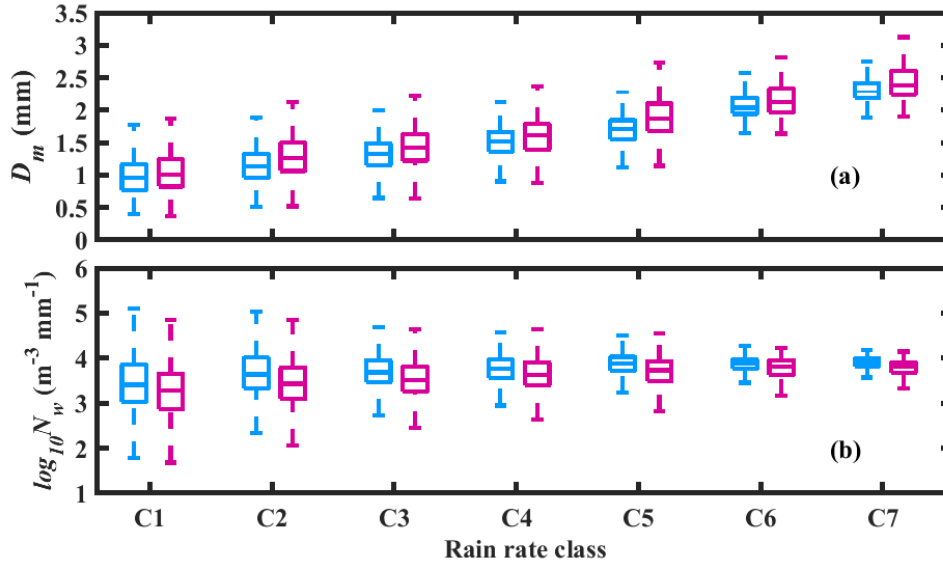
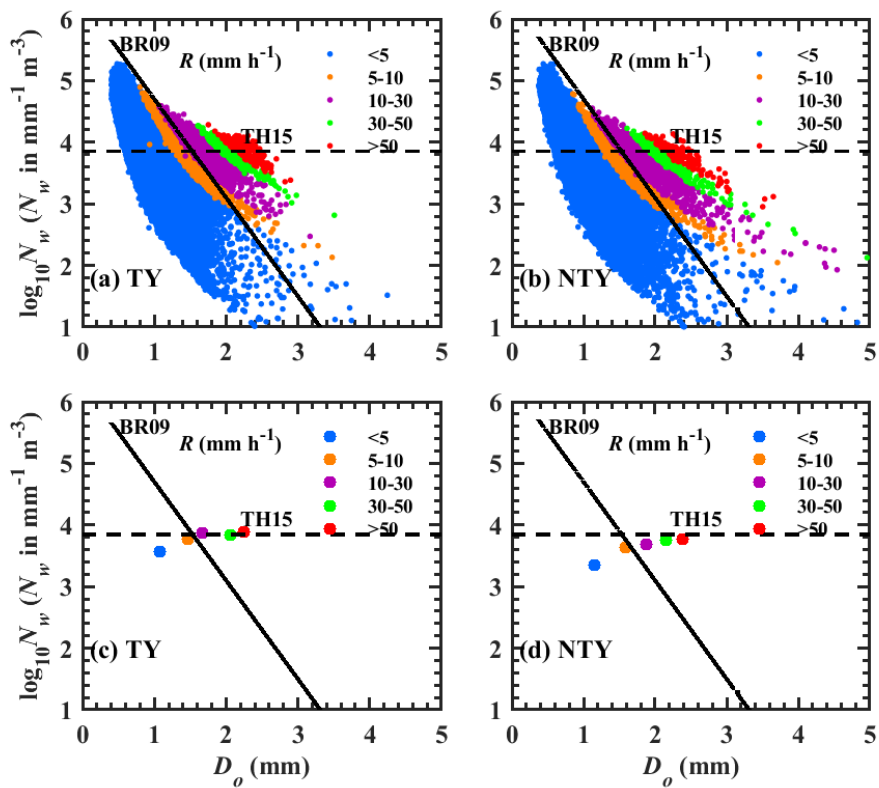


Figure 7. Box plot of (a) D_m (mm) and (b) $\log_{10} N_w$ ($\text{mm}^{-1} \text{m}^{-3}$) in seven rainfall rate classes for typhoon (TY) (sky blue color) and non-typhoon (NTY) (dark magenta color) rainfall. The center line of the box indicates the median, and the bottom and top lines of the box indicate the 25th and 75th percentiles, respectively. The bottom and top of the dashed vertical lines indicate the 5th and 95th percentiles, respectively.



Formatted: Font: (Default) Times New Roman, 12 pt, Bold

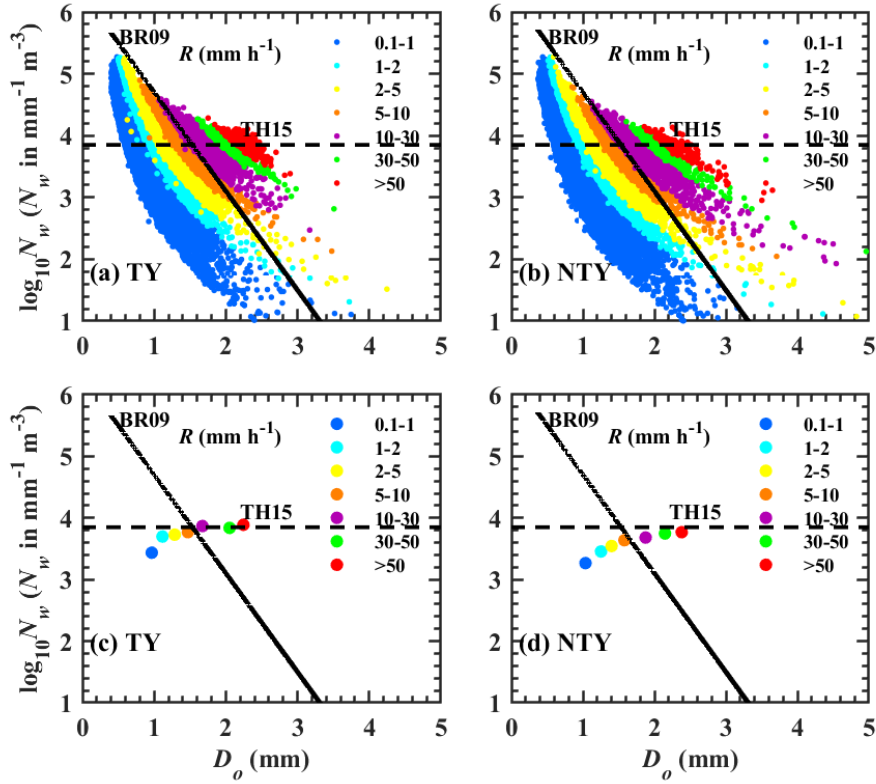


Figure 8. Scatter plots of D_0 - $\log_{10}N_w$ for (a) typhoon (TY) and (b) non-typhoon (NTY) rainfall, mean values of D_0 and $\log_{10}N_w$ for (c) typhoon (TY) and (d) non-typhoon (NTY) rainfall in different rainfall rate ranges. Stratiform and convective precipitation separation line of Thompson et al. (2015): TH15 and Bringi et al. (2009): BR09 are represented, respectively, with horizontal dotted line and inclined solid line.

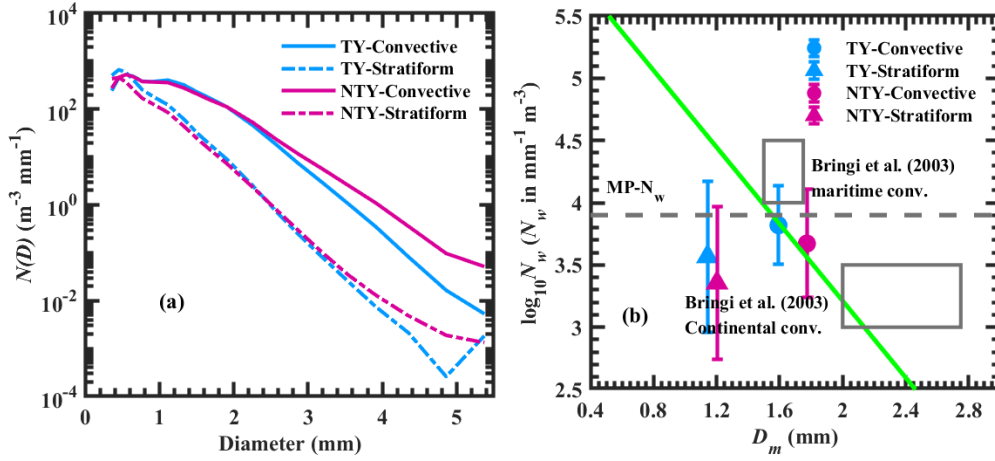
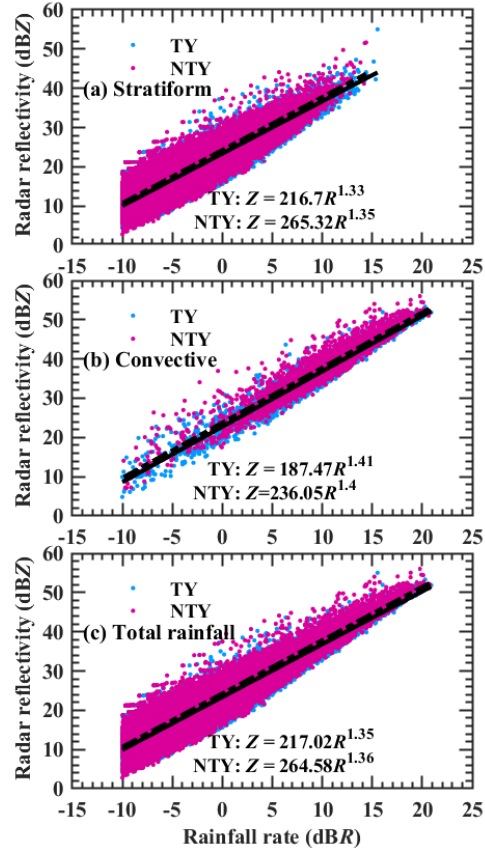


Figure 9. (a) Distribution of $N(D)$ ($\text{m}^{-3} \text{mm}^{-1}$) with raindrop diameter in stratiform and convective precipitation for typhoon (TY) and non-typhoon (NTY) rainfall. (b) Variations of $\log_{10} N_w$ (where N_w is the normalized intercept parameter in $\text{mm}^{-1} \text{m}^{-3}$) with D_m (mass-weighted mean diameter in mm) in stratiform and convective regimes for typhoon (TY) and non-typhoon (NTY) rainfall. The horizontal gray dashed line is the Marshall-Palmer value of $\log_{10} N_w$ (3.9) for exponential shape. The green dash dotted line is the stratiform and convective separation line of Bring et al. (2003).



856
857 **Figure 10.** Scatter plots of radar reflectivity (Z , dBZ) and rainfall rate in logarithmic scale
858 $(10 \cdot \log_{10} R, \text{dBR}, R \text{ in } \text{mm h}^{-1})$ for typhoon (TY) and non-typhoon (NTY) rainfall.

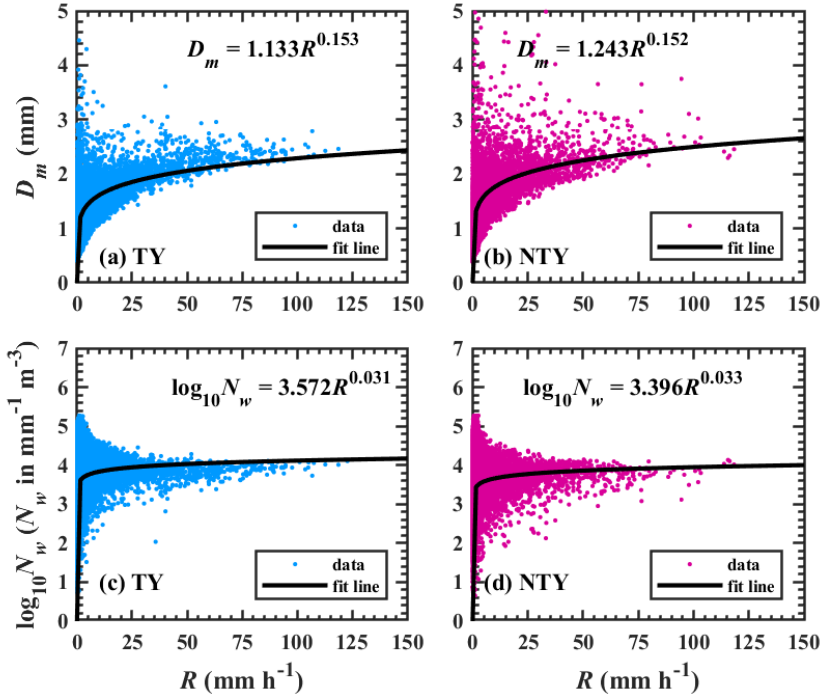


Figure 11. Distributions of D_m (mm) and $\log_{10}N_w$ (N_w in $\text{mm}^{-1} \text{m}^{-3}$) with rainfall rate (R , mm h^{-1}) for typhoon (TY) and non-typhoon (NTY) rainfall.

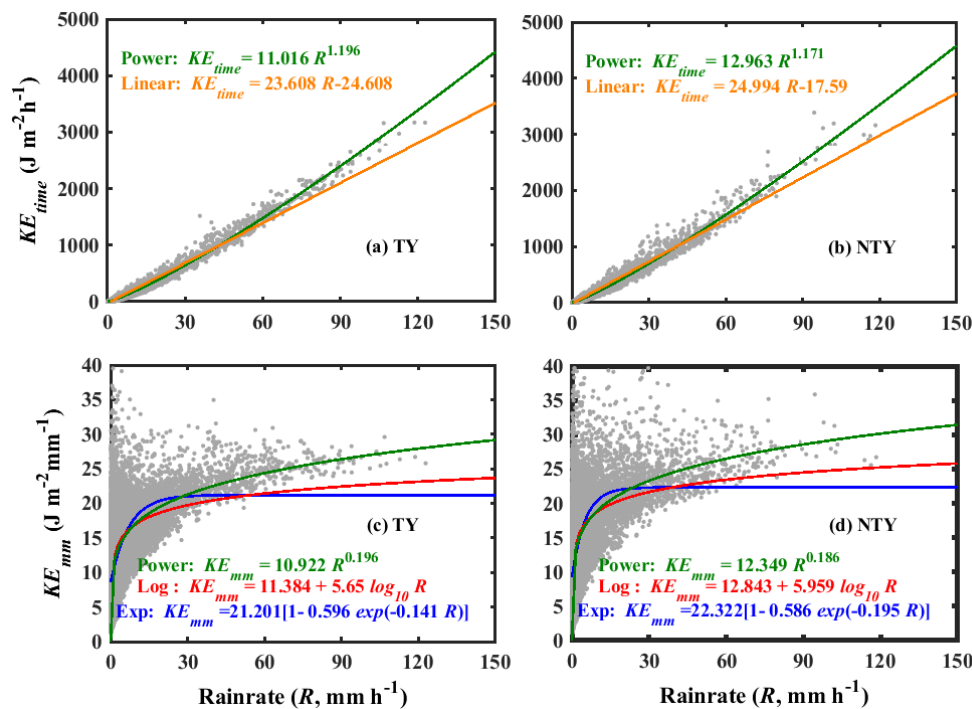
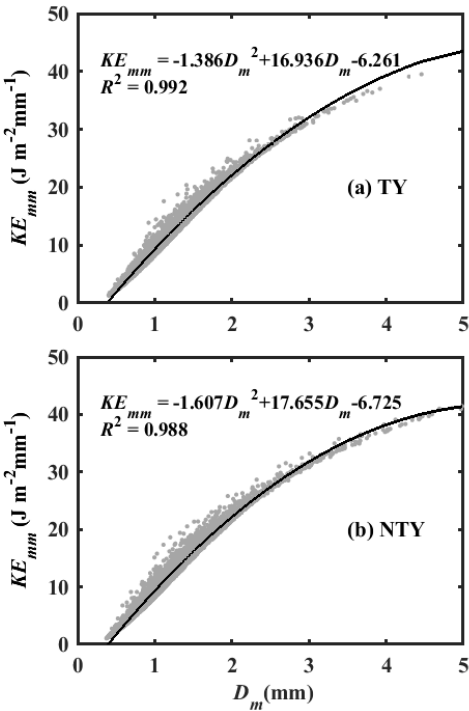


Figure 12. Scatter plots of rainfall kinetic energy (KE) [time-specific KE , KE_{time} ; volume-specific KE , KE_{mm}] with rainfall rate (R , mm h^{-1}) for typhoon (TY) and non-typhoon (NTY) rainfall.

881



882

883 **Figure 13.** Scatter plots of volume-specific KE (KE_{mm} in $\text{J m}^{-2} \text{ mm}^{-1}$] with D_m (mm) for typhoon
884 (TY) and non-typhoon (NTY) rainfall.

885

886

887

888

889

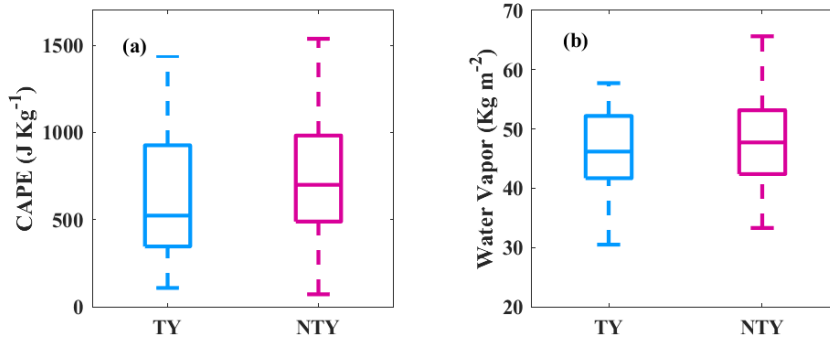


Figure 14: Variations in (a) convective available potential energy (CAPE, J Kg^{-1}) and (b) vertical integral of water vapor (kg m^{-2}) for typhoon (TY) and non-typhoon (NTY) rainfall. The center line of the box indicates the median, and the bottom and top lines of the box indicate the 25th and 75th percentiles, respectively. The bottom and top of the dashed vertical lines indicate the 5th and 95th percentiles, respectively

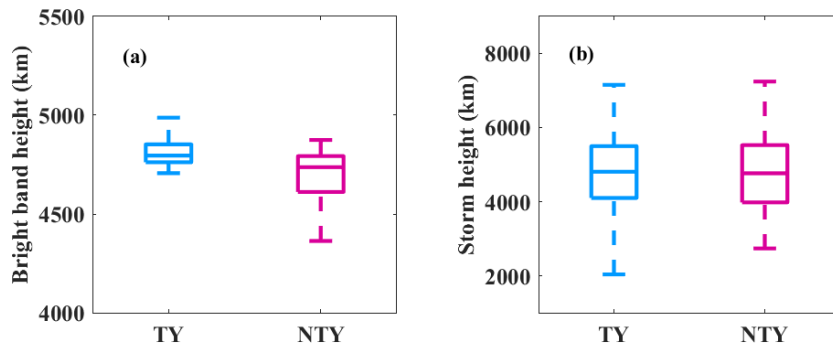


Figure 15. (a) Bright band (BB) and (b) storm heights box plots for typhoon (TY) and non-typhoon (NTY) rainfall.

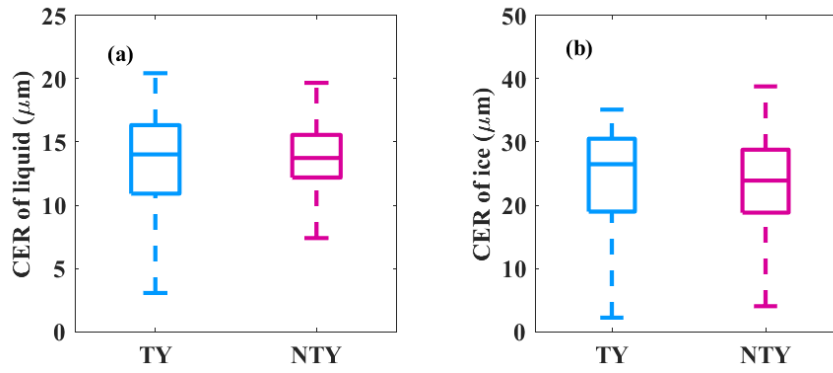


Figure 16. (a) Liquid, (b) ice particles cloud effective radii (CER, μm) values for typhoon (TY) and non-typhoon (NTY) rainfall.

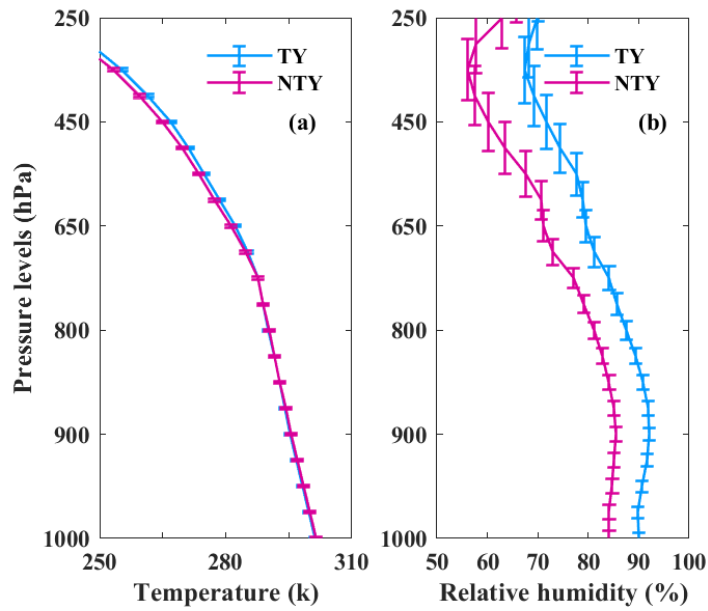
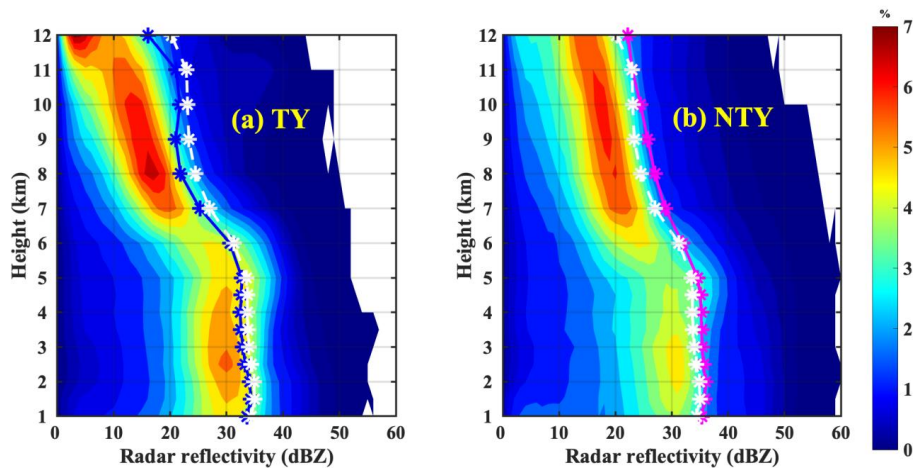
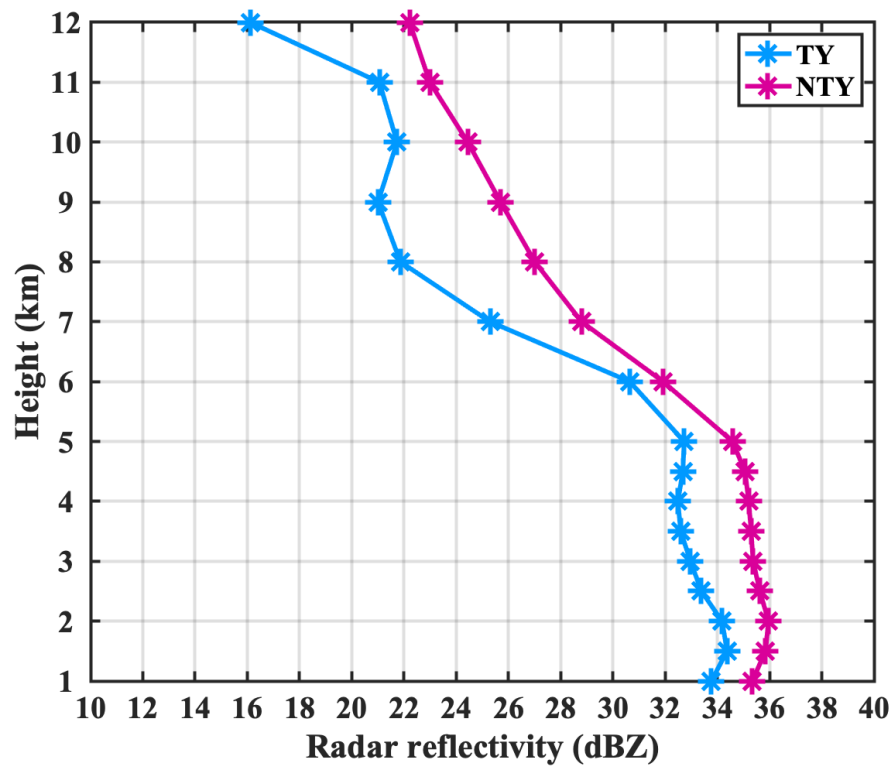


Figure 17. (a) Mean air temperature ($^{\circ}\text{C}$) and (b) relative humidity (%) profiles for typhoon (TY) and non-typhoon (NTY) rainfall.



935
936 **Figure 18.** Radar reflectivity contoured frequency-by-altitude diagram (CFAD) from six ground-
937 based radars for (a) typhoon (TY) and (b) non-typhoon (NTY) rainfall.

938



939

940 **Figure 19.** Mean radar reflectivity profiles of typhoon (TY) and non-typhoon (NTY) rainfall.

941

942